Meteoritics & Planetary Science 33, 581–601 (1998)

Geochemistry and petrology of lunar meteorite Queen Alexandra Range 94281, a mixed mare and highland regolith breccia, with special emphasis on very-low-titanium mafic components

BRADLEY L. JOLLIFF*, RANDY L. KOROTEV AND KAYLYNN M. ROCKOW

Department of Earth and Planetary Sciences and The McDonnell Center for the Space Sciences,
Washington University, St. Louis, Missouri 63130, USA
*Correspondence author's e-mail address: blj@levee.wustl.edu

(Received 1997 June 2; accepted in revised form 1998 March 3)

Abstract–Queen Alexandra Range (QUE) 94281, a lunar meteorite recently discovered in Antarctica, is a glassy-matrix, clast-rich regolith breccia containing a mixture of mafic, volcanic-glass and gabbroic constituents and a diverse set of highland constituents. In thin section, the clast assemblage is dominated by coarse mineral debris from a shallow intrusive or hypabyssal setting, or from deep within a thick mare flow. Abundant coarse-grained pyroxene clasts have fine-scale exsolution lamellae and compositions similar to pyroxenes of known lunar very-low-Ti (VLT) basalts and other lunar meteorites of basaltic composition. Pyroxene compositions follow Fe-enrichment extending to hedenbergite, which is associated with fayalite and cristobalite, indicating slow cooling. We refer to the protolith of the crystalline VLT component as VLT gabbro. Fragments of pyroclastic glasses that have high Fe and low Ti concentrations, similar to the pyroclastic green glasses known from Apollo samples, are common. Lithic clasts include abundant subrounded, glassy to cryptocrystalline, aluminous (~17–30 wt% Al_2O_3) KREEP-poor melt breccias of highland origin and a variety of other feldspathic impactites. On the basis of composition of our subsamples, QUE 94281 consists of ~54 wt% mafic or "mare" components and 46 wt% feldspathic or "highland" components.

The bulk composition of QUE 94281 is similar to that of Yamato (Y) 793274, but QUE 94281 has slightly greater concentrations of some siderophile elements and slightly lower concentrations of those elements contributed mainly by mafic constituents. Differences in siderophile element concentrations are consistent with longer surface exposure of QUE 94281. Minor differences in trace element variations of subsamples of the two meteorites suggest subtle differences in the composition of their highland constituents. Nonetheless, the overall similarity of compositions supports the possibility that they were ejected from the same source region on the Moon.

The crystalline VLT component of QUE 94281 differs from those known from Apollo 17 and Luna 24 VLT lithologies and from that of basaltic breccia Elephant Moraine (EET) 87521. The VLT-gabbro component and the ferroan VLT volcanic glasses in QUE 94281 have compositions that may be petrogenetically related by derivation from a common picritic parent composition, represented by an ultramafic glass found in QUE 94281.

INTRODUCTION

Of the thirteen lunar meteorites discovered and reported to date, eight are relatively feldspathic, with Al_2O_3 concentrations >20 wt%: ALHA81005, Calcalong Creek, MAC 88104/5, QUE 93069/QUE 94269 (see Eugster and Polnau, 1996, for pairing), Yamato 791197, Yamato 892192, Yamato 86032, and Dar Al Gani 262 (Bischoff and Weber, 1997); and five are relatively mafic, with Al_2O_3 concentrations <18 wt%: Asuka (A) 881757, EET 87521, QUE 94281, Yamato 793169, and Yamato 793274. Among the mafic lunar meteorites, compositions of basaltic components are similar to the compositions of low-Ti mare basalts (Y-793169 and A-881757, Lindstrom *et al.*, 1991a; Warren and Kallemeyn, 1993; Koeberl *et al.*, 1993; Jolliff *et al.*, 1993) or very-low-Ti (VLT) mare basalts (EET 87521, Warren and Kallemeyn, 1991; Y-793274, Lindstrom *et al.*, 1991b; and QUE 94281, Lindstrom *et al.*, 1996). The preponderance of low-Ti to very-low-Ti mare components in the Antarctic lunar meteorites contrasts with the compositional distribution of mare basalts returned by the Apollo missions, which mostly have moderate to high Ti concentrations, but is consistent with results of remote sensing, which indicate that low-Ti basalts may be widespread in some of the maria (Pieters, 1978). Queen Alexandra Range 94281 bears petrographic and compositional similarities to other lunar meteorites (EET 87521 and Y-793274), which suggests that they all might come from the same region of the Moon (Warren, 1994; Arai *et al.*, 1996; and addressed herein); however, this 23 g meteorite provides additional clues to the nature of that region, which differs significantly from regions explored by Apollo missions.

Preliminary reports on QUE 94281 described it as a regolith breccia rich in glass and mineral clasts, consisting of a mixture of mainly mafic, presumably mare components, and some highland components (Arai *et al.*, 1996; Jolliff *et al.*, 1996a; Kring *et al.*, 1996; and Lindstrom *et al.*, 1996). Compositionally, QUE 94281 is most similar to Y-793274 (Eugster and Polnau, 1996; Jolliff *et al.*, 1996a; Lindstrom *et al.*, 1996; Dreibus *et al.*, 1996), and compositions and textures of mineral clasts are similar to those observed in Y-793274 and EET 87521 (Arai *et al.*, 1996; Jolliff *et al.*, 1996a). From preliminary investigation, the noble gas contents of QUE 94281 do not support pairing with Y-793274 (Eugster and Polnau, 1996); however, Warren and Arai (1997) suggested pairing based on a comparison of the compositions of pyroclastic glasses and bulk-rock Cr and V trends. Cosmogenic nuclides reflect a complex exposure history for QUE 94281 involving cosmic-ray exposure both at the surface of the Moon and during transport from the Moon to the Earth (Nishiizumi and Caffee, 1996).

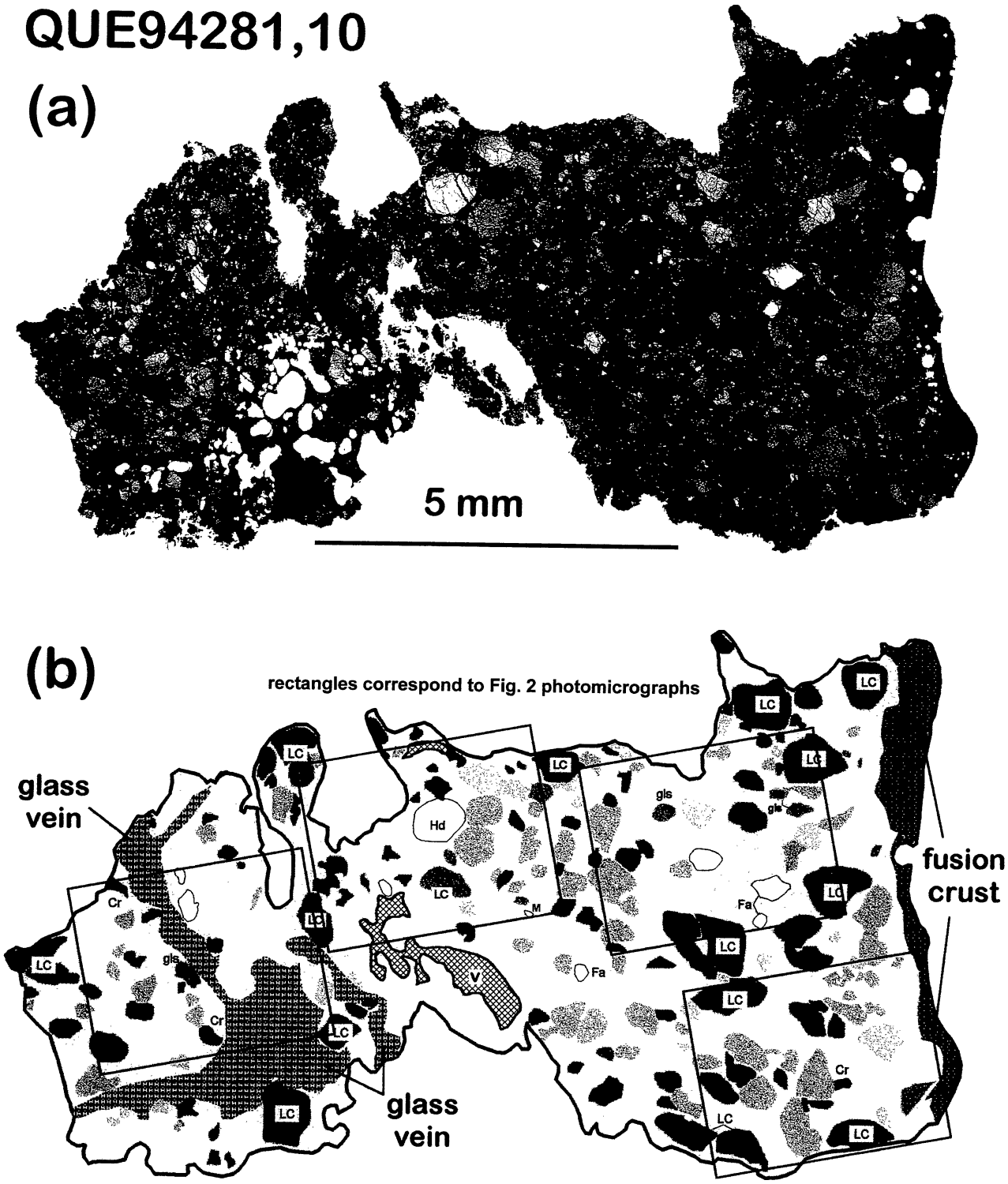

FIG. 1. (a) Backscattered electron image (BEI) mosaic of QUE 94281,10. Materials having the highest mean atomic number appear brightest. These include one small grain of Fe-Ni metal, fayalite, and hedenbergite. Most of the dark gray clasts are plagioclase, but several that appear to be black are cristobalite. White ovoid areas within glass of the fusion crust (right edge) and the interior glass vein (lower left) are vesicles or voids. (b) Line drawing of major constituents, including all clasts >500 μm. Clasts are shown in shades of gray corresponding approximately to their brightness in the BEI of part (a). Void areas within the breccia are marked by a crosshatched pattern. Abbreviations: LC = lithic clast; gls = glass clast; Fa = fayalite; Hd = hedenbergite; Cr = cristobalite; M = metal; v = void. Areas enclosed by rectangles are shown in Fig. 2.

In this paper, we present the results of our investigation of QUE 94281 based on petrographic observations and electron-microprobe analysis (EMPA) of thin section 94281,10. We report compositional analyses by instrumental neutron activation analysis (INAA) of small chips of the meteorite, including typical breccia and fusion crust glass, and we report the major element compositions by EMPA of the largest mineral clasts, a suite of lithic and glass clasts, glass of the fusion crust, and a glassy vein that transects the thin section. We compare the compositions of components in QUE 94281 to those of other similar Apollo materials and lunar meteorites.

SAMPLES STUDIED AND ANALYTICAL METHODS

Samples Studied

We received for study four subsamples of QUE 94281, each consisting of fragments, and a thin section, QUE 94281,10. The four primary subsamples (QUE 94281,33, 34, 35, and 36) were further subdivided by carefully breaking them into smaller fragments or by gently crushing them. Dust from breaking or crushing was removed from the larger fragments by an ultrasonic rinse in acetone prior to analysis by INAA.

Subsample 33 was of glassy breccia, termed "chaotic material" by the curator, and consisted initially of 11 fragments plus fines material. We analyzed the seven largest fragments individually and crushed and combined the remaining ones into a composite sample. This composite was split by magnetic separation to create three subsamples enriched in different mineral and glass components. The most magnetic split (MS3) proved to be rich in material containing extralunar meteoritic metal, and the split of intermediate magnetic susceptibility was rich in pyroxene.

Subsample 34 was dark, massive, conchoidally fractured glass. The original fragment appeared to contain a slightly lighter glass attached or "welded" to the black glass; this we removed as subsample 34A. The massive black glass fragments were further subdivided into four additional subsamples, B–E, to test for homogeneity.

Subsample 35 consisted of coherent, angular fragments of bulk breccia, mostly containing clasts too small to separate without microdrilling. One 27.2 mg fragment contained a fractured and friable white clast that appeared under the binocular microscope to be a granulitic breccia. This fragment was broken and designated as subsamples 35A1 (mostly fragments of the clast) and 35A2 (clasts plus matrix). The remaining large fragments were analyzed individually (B–D) and the crumbs and fines were combined (E). The rationale for analyzing similar breccia subsamples is that minor variations in composition, if present, can be used to infer the compositions of different components that make up the breccia.

Subsample 36 was also of bulk breccia but contained some exterior glass. This subsample originally contained three large fragments (A, B, C), which we further subdivided to increase the likelihood of measuring compositional variability on a small scale. All were very coherent and had no large, separable clasts. Brief descriptions of each subsample are given as part of Table A1 (appendix) along with the corresponding chemical composition by INAA.

Electron-Microprobe Analysis

We used a JEOL 733 Superprobe equipped with a backscattered-electron detector, three wavelength-dispersive spectrometers, and Advanced Microbeam automation for electron-microprobe analysis. For quantitative mineral and glass analyses, an accelerating voltage of 15 kV was used with a 20 nA beam current for plagioclase, a 30 nA beam current for mafic silicates, and beam diameters ranging from 1–40 μm, depending on the target. Large beam diameters were used to integrate exsolved pyroxene grains to obtain bulk pyroxene analyses. Smaller beam diameters were used to analyze host pyroxene and exsolution lamellae. We used beam diameters of 10–30 μm for glass and plagioclase analyses to avoid Na volatilization. We used a combination of silicate and oxide mineral standards and silicate glass standards. X-ray matrix corrections were based on a modified Armstrong (1988) CITZAF routine incorporated into the electron microprobe software.

Instrumental Neutron Activation Analysis

Procedures were similar to those described by Korotev (1991, 1996a), with the following specifics. Samples and standards were irradiated together for 48 h at a thermal-neutron flux of 5.15×10^{13} cm^{-2}s^{-1}. Samples received 3 or 4 radioassays beginning 5–6 days following the irradiation.

RESULTS

Petrographic Description

Thin section QUE 94281,10, a rock slice of irregular shape ~5 mm × 12 mm (Fig. 1), contains clast-rich breccia with a maximum grain size of ~1 mm, a highly vesicular glass vein, and a thin fusion crust, ranging up to ~0.5 mm thick (Figs. 1 and 2). The breccia is dominated by abundant mineral, glass, and lithic clasts, including relatively coarse-grained (up to 0.8 mm grain size) pyroxene and plagioclase clasts, set in a glassy matrix; the proportion of clasts >100 μm is ~35%. The presence of fragments of glass spheres and ellipsoids (Fig. 2b,c) indicates that the meteorite is a regolith breccia. The abundance of mafic, presumably mare-related clastic materials plus the presence of a substantial proportion of highland materials (Figs. 2 and 3) suggest derivation from regolith at a mare-highland interface. Some of the highland materials are evident as clasts of feldspathic glasses and impact-melt breccias (Figs. 1 and 2b), but other nonmare lithic types are also present (Fig. 3e,f). A regolith origin is consistent with cosmogenic nuclides and noble gas data, which indicate a significant residence time at the lunar surface for components of QUE 94281 (Nishiizumi and Caffee, 1996; Eugster and Polnau, 1996). The large interior, vesicular glass vein (Fig. 1; see also Score *et al.*, 1995) is not fractured, suggesting formation when the rock was ejected from the Moon.

The largest clasts consist of individual grains of pyroxene but also include individual grains of plagioclase, olivine, glass, and lithic (polymineralic) clasts. Using a composite backscattered electron image coupled with image processing, the volumetric proportions of clasts ≳100 μm maximum dimension are found to be approximately: lithic clasts, 13.5%; pyroxene, 12%; plagioclase, 6%; olivine, 1%; and cristobalite, 0.5%. The remainder, excluding glass and vesicles of the interior vein and of the fusion crust, constitutes some 65%, which we designate matrix.

One of the most striking features of this new lunar sample is the abundance of relatively coarse-grained (up to 0.8 mm grain size) exsolved pigeonite and ferroaugite fragments (Figs. 1, 2a, 3a–d). Individual grains are only moderately zoned in composition, typically contain fine (001) lamellar exsolution, with individual lamellae ≤5 μm and typically 1–2 μm (Fig. 3c,d). Together, these grains define compositional trends (Figs. 4 and 5) similar to those of pyroxenes of slowly cooled Luna 24 VLT basalts (Papike and Vaniman, 1978), and generally similar to pyroxenes of Y-793274 (Takeda *et al.*, 1991a,b; Yanai and Kojima, 1990, 1991), Y-793169 (Yanai and Kojima, 1990, 1991), A-881757 (Yanai and Kojima, 1990), and EET 87521 (Delaney, 1989). Coarse pyroxene grains have compositions

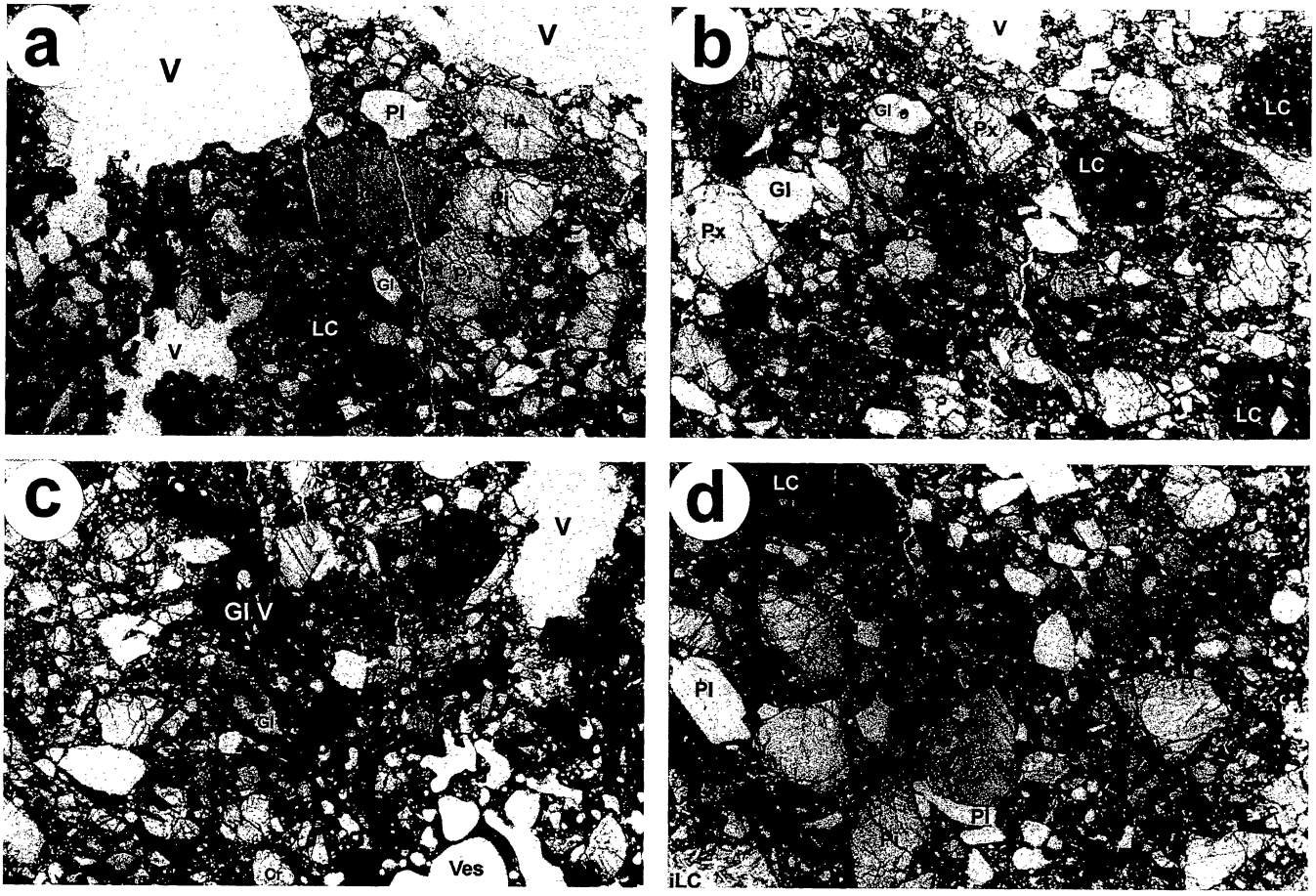

FIG. 2. Transmitted light photomicrographs of clasts in QUE 94281. Locations of photos on thin section QUE 94281,10 are shown in Fig. 1b. Each photomicrograph is ~3.3 mm across. Void areas, filled by epoxy, are shown by "V." (a) Cluster of coarse pyroxene clasts (right-center) includes coarse hedenbergite (Hd), ferroaugite (FA), and pigeonite (Pi); see also Fig. 3a. Dark areas in the matrix include glass and glassy-matrix lithic clasts, including a mafic lithic clast (LC, bottom center). Clear, colorless clasts include plagioclase (Pl, above the hedenbergite grain) and glass (Gl, below the hedenbergite grain). (b) Mineral, glass, and lithic clasts: shocked, partially melted pyroxene clast (sh Px, upper left); pyroclastic glass with a small vesicle (Gl, upper left center); dark, glassy-matrix lithic clasts (LC, center, upper and lower right). (c) Dark, glassy vein (pseudotachylite) traversing from upper left to lower center (Gl V), and highly vesiculated part of vein (Ves, along lower right). Along left side of dark glass vein is a fragment of a pyroclastic glass bead (Gl). A relatively coarse cristobalite grain (Cr) occurs along the bottom edge of the photo. (d) Mineral and lithic clasts, including a polygrain aggregate or glomerocryst of pigeonite (Pi) and plagioclase (Pl) in the lower-central area, dark, glassy-matrix breccia (LC, upper left), and a fine-grained, intergranular lithic clast (iLC, lower left, see also Fig. 3f).

ranging in *Mg'* from ~70 to <20 (Fig. 4) and Ti/(Ti + Cr), from ~0.2 to 1.0 (Fig. 5). On close comparison, however, pyroxenes in EET 87521 and A-881757 are restricted to more Fe-rich compositions than QUE 94281 pyroxenes (Yanai and Kojima, 1991, their Fig. 5b). Bulk compositions of coarse pyroxene grains (Table A2), obtained by EMP analysis using a broad electron-beam diameter relative to the width of exsolution lamellae, indicate crystallization temperatures beginning ~1200 °C and extending to ~1000 °C (Fig. 6a).

Coarse plagioclase clasts have An contents of 87–95, lower than those from Apollo 17 and Luna 24 VLT basalts (An > 90) but similar to those in other mafic lunar meteorites. Polymineralic clusters of pyroxene, plagioclase, and in some cases olivine (*e.g.*, Fig. 2d), in which mineral compositions are similar to those of single-mineral clasts, provide evidence that many of the coarse mineral clasts are related to each other through a common parent lithology. Compositions of coexisting coarse mineral clasts are listed in Tables A3 (plagioclase) and A4 (olivine), where compositions of individual grains are cross-referenced to compositions of coexisting pyroxenes (A2).

Relatively coarse grains (measuring hundreds of micrometers) of hedenbergite, fayalite, and cristobalite, as well as fine-grained intergrowths of these minerals (Fig. 3b) occur among the clasts; these assemblages indicate strong differentiation but slow cooling. Similar assemblages were also observed in Y-793274 (Takeda *et al.*, 1991b). More rapidly cooled ferrobasaltic rocks develop metastable pyroxferroite rather than hedenbergite and fayalite (Papike and Vaniman, 1978); we observed no pyroxferroite in this sample. On the other hand, deep plutonic rocks containing pigeonite cool slowly enough for pigeonite to invert, but we observe no inverted pigeonite in QUE 94281. On the basis of exsolved pyroxene compositions, measured with a 1–2 μm electron beam, equilibration temperatures extend no lower than ~900 °C (Fig. 6b), which is consistent with relatively shallow depth of crystallization.

In addition to mineral clasts, QUE 94281 contains a diverse assortment of lithic clasts and glasses. The lithic clasts include glassy and cryptocrystalline, subrounded impact-melt breccias that range from mafic to feldspathic (see below for compositions). A

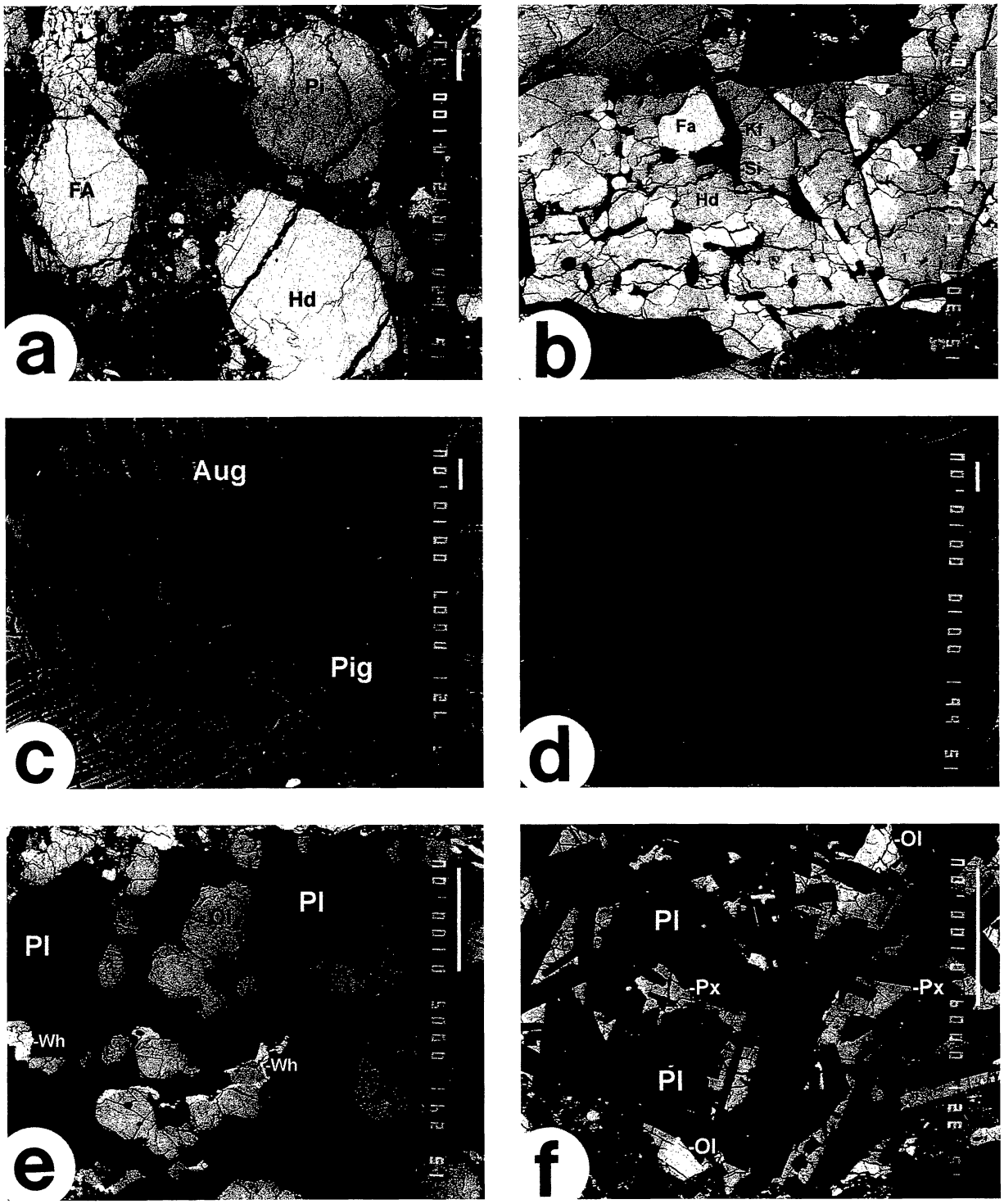

FIG. 3. Backscattered electron images of clasts in QUE 94281,10. (a) Coarse pyroxene clasts; field of view ~1.5 mm. Brightness mainly reflects the degree of Fe-enrichment. The larger bright grain is hedenbergite (Hd) and the smaller bright grain is ferroaugite (FA). Others are pigeonite (Pi). The field of view is rotated ~90° counterclockwise from that of Fig. 2a. (b) Fine-grained eutectoid assemblage, in order of brightness, of fayalite (Fa, white), hedenbergite (Hd, light gray and constituting most of the assemblage), K-feldspar (Kf, dark gray), and silica (Si, black); scale bar is 100 μm. (c) and (d) Finely exsolved pyroxene grains; light gray is low-Ca pyroxene, dark-gray is high-Ca pyroxene. Grain shown in (c) is composite, with part augite host (Aug) and part pigeonite host (Pig). Scale bars are 10 μm. Note offsets and translation of lamellae along fractures and microfaults. (e) Fine-grained, strongly fractured, plagioclase-rich granulite containing small olivine grains (Ol, light gray) and whitlockite (Wh, bright) (see Table A5). Scale bar is 100 μm. (f) Fine-grained, plagioclase-rich, intergranular lithic clast (see Table A5). Most of the intergranular spaces are filled by pyroxene (Px, light gray, conformed by the shape of plagioclase grains) and some olivine (Ol, bright). Scale bar is 100 μm.

partially annealed, feldspathic granulite (Table A5, lithic clast 1) contains plagioclase (An_{94}), fine-grained, equant olivine grains (Fo_{70}), and interstitial RE-whitlockite (Fig. 3e). A plagioclase-pyroxene-olivine-ilmenite assemblage (Table A5, lithic clast 2) contains magnesian mafic minerals ($Mg' \approx 80$) and An_{94} plagioclase but also contains An_{63} plagioclase, which indicates that it is a polymict breccia. A fine-grained, intergranular feldspathic basalt (Table A5, lithic clast 3) contains plagioclase (An_{95}), olivine (Fo_{63}), and calcic pyroxene ($Wo_{37}En_{50}Fs_{13}$) and is probably a melt-rock clast (Fig. 3f). Small, elliptical glass clasts and broken fragments (*e.g.*, Fig. 2b,c), which are typically light green in thin section, have Fe-rich and Ti-poor compositions that are similar to members of the green volcanic-glass suite (*e.g.*, Steele *et al.*, 1992) but differ mainly in higher Al, Ca, and Na concentrations than VLT volcanic glasses in the Apollo samples (see below).

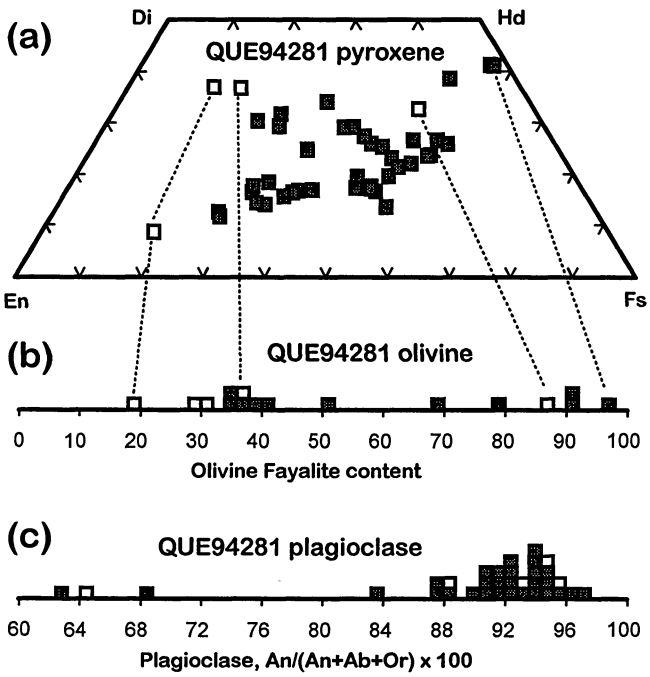

FIG. 4. Compositions of pyroxene, olivine, and plagioclase in QUE 94281. Filled symbols are for individual, coarse-grained mineral clasts, and open symbols are for minerals in lithic clasts. Dashed lines connect coexisting pyroxenes and olivines. (a) Pyroxene quadrilateral; compositions are "corrected" for nonquadrilateral components (see Table A2). Compositions of individual pyroxene clasts (filled squares) are broad-beam composite analyses, not individual lamellae, of representative grains among the coarsest clasts. (b) Olivine fayalite contents (atomic Fe/(Fe + Mg)). (c) Plagioclase An content of coarse plagioclase clasts and plagioclase in lithic clasts.

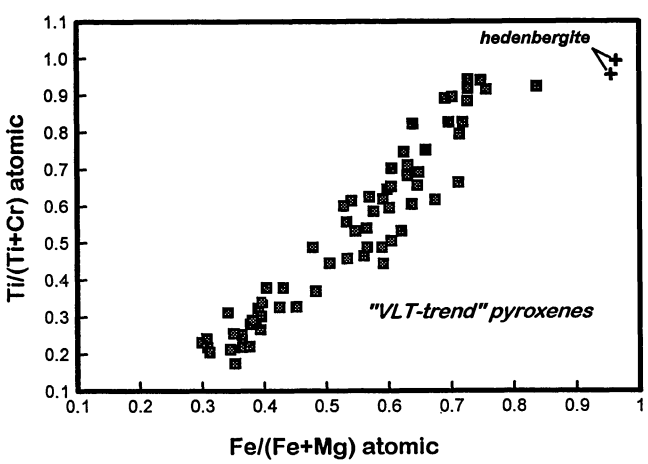

FIG. 5. Fe/(Fe + Mg) *vs.* Ti/(Ti + Cr) for coarse pyroxene clasts in QUE 94281. Compositions lie along a single trend related to magmatic differentiation, beginning with relatively magnesian, Ti-poor compositions and extending to ferroan, Ti-rich compositions. This trend is similar to that of other VLT lunar basalts (see text).

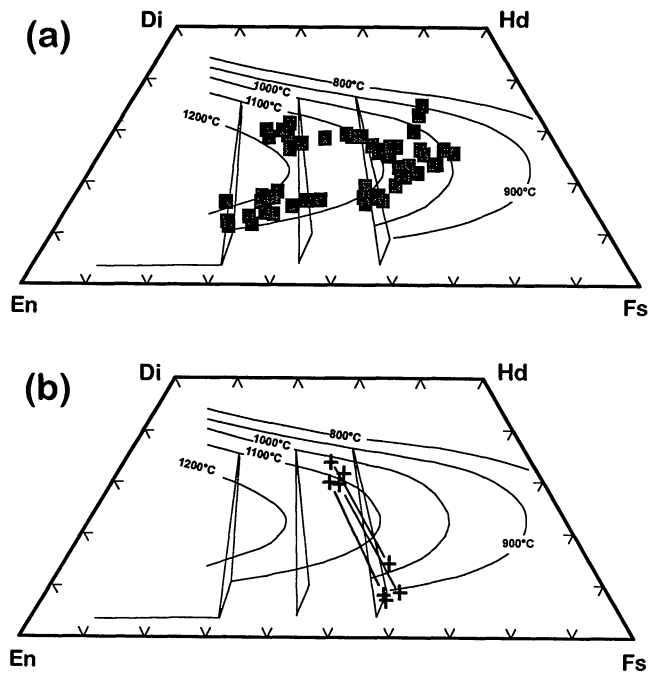

FIG. 6. Pyroxene quadrilateral compositions for the "VLT-trend" mineral clasts superimposed on the two-pyroxene thermometer of Lindsley and Anderson (1983). (a) Bulk analyses (incorporating both host and exsolution lamellae) follow roughly, and lie between, the 1200 °C and 1000 °C isotherms. These pyroxene compositions appear to relate the mineral clasts to one another and follow a slow cooling trend, leading to the assemblage fayalite-hedenbergite-cristobalite. A break in the differentiation trend from magnesian to ferroan pyroxene compositions at about $Mg' = 50$ may correspond to a hiatus in the crystallization interval at ~1125 °C. (b) Compositions of coexisting host-lamellae pairs, showing equilibration temperatures. Compositions of low-Ca hosts suggest equilibration to at least 900 °C. The compositions of thin, high-Ca pyroxene lamellae may be compromised by beam overlap onto low-Ca hosts, thus indicating equilibration temperatures that are too high.

Bulk and Constituent Chemical Compositions

Table 1 lists the major element compositions of several materials found in QUE 94281: the fusion crust, an interior glass vein, an average of mafic glasses, and an average of feldspathic impact-melt clasts. Table 2 lists trace element compositions of subsamples of the four primary splits analyzed by INAA; these represent the fusion crust (QUE 94281,34, column 1), breccia (QUE 94281,33 and 34, columns 2 and 3), and glass plus breccia (QUE 94281,36, column 4).

We might expect the fusion crust and the interior glass vein to represent bulk-meteorite melts. Indeed, the weighted mean composition of all subsamples analyzed by INAA (Table 2, "grand mean") is similar to the composition of the fusion crust (Table 1) as determined by both INAA and EMPA for those elements analyzed by both techniques. However, there is a hint of some variability of composition of the fusion crust glass. One of the subsamples of QUE 94281,34 (subsample A, Table A1) is visibly lighter in color

TABLE 1. Major element compositions of lithologic constituents of the QUE 94281 lunar meteorite.

	Fusion Crust		Glass Vein		Mafic Glasses		Feldspathic Clasts		Y-793274
	mean (5)	ssd	mean (8)	ssd	mean (8)	ssd	mean (9)	ssd	Lit Avg.
SiO_2	45.6	0.3	45.2	0.3	45.5	1.3	45.1	1.2	47.0
TiO_2	0.59	0.02	0.50	0.04	1.15	1.5	0.49	0.35	0.58
Al_2O_3	17.2	0.9	19.9	0.3	10.5	1.6	26.5	3.5	16.1
Cr_2O_3	0.26	0.03	0.25	0.03	0.46	0.14	0.11	0.08	0.26
FeO	12.9	0.7	11.0	0.3	18.7	1.4	5.89	2.5	14.1
MnO	0.18	0.01	0.15	0.02	0.24	0.03	0.08	0.05	0.16
MgO	9.61	0.3	10.1	0.1	13.4	3.6	6.09	2.4	9.12
CaO	12.3	0.05	12.5	0.09	9.7	1.4	14.8	1.4	12.2
Na_2O	0.45	0.05	0.50	0.02	0.22	0.07	0.48	0.12	0.40
K_2O	0.11	0.09	0.08	0.01	0.02	0.02	0.08	0.05	0.08
P_2O_5	0.06	0.01	0.08	0.01	0.04	0.05	0.06	0.09	0.08
Sum	99.3		100.3		99.9		99.7		100.1
*Mg'	57.1		62.1		56.1		64.8		53.6

*Mg' = molar MgO/(MgO + FeO) × 100. Oxides given in weight percent, determined by EMPA. All iron reported as FeO. The number of analyses used to calculate each mean is given in parentheses and ssd is the *sample* standard deviation. The bulk composition of Y-793274 is an average of data from the literature, including Fukuoka (1990), Lindstrom *et al.* (1991b), Koeberl *et al.* (1991), Warren and Kallemeyn (1991), and Yanai and Kojima (1991).

TABLE 2. Chemical composition by instrumental neutron activation analysis of subsamples of QUE 94281.

	Fusion Crust		Interior Breccia				Glass + Breccia		QUE 94281		Y-793274	EET 87521
	QUE 94281,34[1]		QUE 94281,33[2]		QUE 94281,35[3]		QUE 94281,36[4]		grand mean[5]		Lit Avg.[6]	Lit Avg.[7]
	mean	ssd	mean	ssd	mean	ssd	mean	ssd	mean	ssd		
FeO	13.3	0.3	14.0	1.0	12.7	4.2	12.6	0.7	13.2	2.0	14.1	18.8
CaO	12.8	0.6	12.5	0.4	12.5	1.2	13.0	0.4	12.7	0.7	12.2	11.6
Na_2O	0.39	0.03	0.39	0.03	0.41	0.09	0.41	0.02	0.40	0.04	0.40	0.42
K_2O	0.14	0.11	0.11	0.08	0.08	0.04	0.13	0.04	0.12	0.07	0.08	0.06
Sc	29.0	1.5	29.9	3.1	27.4	9.5	27.2	2.2	28.4	4.8	32.5	42.3
Cr	1709	137	1941	116	1560	454	1758	176	1764	265	2055	1674
Co	47.9	3.3	49.8	6.1	35.5	12.1	44.9	9.7	45.3	9.6	43.1	48
Ni	364	78	344	167	131	36	313	204	300	166	103	37
Rb	6.0	1.2	4.9	1.3	5.3	1.1	4.6	1.9	5.1	1.5	<2	nr
Sr	128	17	111	16	128	29	114	25	119	22	120	115
Zr	122	8	89	32	123	35	81	17	100	32	90	122
Cs	0.09	0.02	0.07	0.04	0.10	0.03	0.09	0.04	0.09	0.04	0.1	0.04
Ba	81	10	74	9	87	29	72	9	78	16	61	78
La	7.39	0.43	6.34	0.63	7.63	2.18	6.18	0.45	6.77	1.20	6.07	8.2
Ce	19.9	1.1	16.9	1.6	20.2	5.7	16.6	1.1	18.1	3.2	15.9	20.5
Nd	12.0	1.2	9.2	1.9	11.1	3.9	8.7	1.3	10.0	2.5	10.4	12.7
Sm	3.51	0.21	3.02	0.25	3.56	0.97	2.95	0.21	3.21	0.54	2.80	3.77
Eu	0.86	0.01	0.81	0.05	0.91	0.19	0.85	0.03	0.85	0.10	0.86	0.97
Tb	0.74	0.05	0.65	0.04	0.74	0.16	0.63	0.07	0.68	0.09	0.60	0.82
Yb	2.65	0.15	2.35	0.14	2.68	0.47	2.26	0.14	2.45	0.30	2.41	3.02
Lu	0.368	0.021	0.327	0.017	0.377	0.067	0.315	0.019	0.342	0.042	0.34	0.44
Hf	2.60	0.15	2.28	0.22	3.32	0.74	2.25	0.22	2.54	0.56	2.37	2.75
Ta	0.32	0.02	0.29	0.03	0.44	0.17	0.30	0.08	0.33	0.10	0.29	0.33
Ir (ppb)	12.7	4.3	12.0	6.1	5.6	3.2	10.4	6.5	10.5	5.9	4.7	0.3
Au (ppb)	2.0	1.2	3.9	1.8	1.5	1.4	3.0	1.7	2.8	1.8	2.9	0.1
Th	1.14	0.06	0.95	0.10	1.21	0.34	0.96	0.08	1.04	0.20	0.88	0.97
U	0.29	0.04	0.25	0.06	0.31	0.09	0.24	0.03	0.27	0.07	0.21	0.25
mass (mg)	88.0		115.5		73.5		115.2		392.2			

Oxides given in weight percent, all others in ppm, except as noted. All iron reported as FeO. Averages for K_2O, Rb, Cs, and Nd based on low concentration values with relatively high uncertainties (see Table A1). Means are mass-weighted and "ssd" is the unweighted *sample* standard deviation: [1]QUE 94281,34 = fusion crust, five subsamples; [2]QUE 94281,33 = interior breccia, seven subsamples; [3]QUE 94281,35 = interior breccia, including ITE-rich clast, six subsamples; [4]QUE 94281,36 glass + breccia, seven subsamples; [5]Grand mean of all subsamples excluding magnetic separates; [6]Y-793274 composition is an average of data from Fukuoka (1990), Lindstrom *et al.* (1991b), Koeberl *et al.* (1991), and Warren and Kallemeyn (1991). Note that concentration values for Y-793274 lie within the ssd for the QUE 94281 grand mean for nearly all elements. [7]Composition of EET 87521 is an average of two compositions given by Warren and Kallemeyn (1991); nr = not reported.

than the others and has a smooth contact with the thicker black glass. Subsample 34A has Na_2O = 0.44 wt% *vs.* 0.36–0.39 wt% for the others (Table A1). Furthermore, as measured by EMPA, the narrow fusion crust on the thin section has 0.45 wt% Na_2O (Table 1). The cause of these variations in Na_2O concentration is unclear and may be related to variable volatilization rather than to differences in what was melted. Other major element concentrations differ slightly but significantly between 34A and the other subsamples analyzed by INAA, including CaO and FeO, and are similar between 34A and the fusion crust that we analyzed in thin section. Nevertheless, relative to other components in the meteorite, including the interior glass vein, the compositions of fusion crust subsamples are very similar to each other. We consider the fusion crust composition to be a good approximation of the bulk composition of the meteorite (Korotev *et al.*, 1996, made a similar assumption for QUE 93069).

The composition of the vesicular, interior glass vein differs from that of the black glass of subsample 34; it is significantly more aluminous, slightly more magnesian, and poorer in iron (Table 1 and Fig. 7a,b). In fact, its FeO concentration is significantly less (11.0 ± 0.3 wt%) than the weighted mean composition of all subsamples combined (the bulk composition), as determined by INAA (13.2 wt%). Thus, it appears that the interior glass vein is a fine-scale pseudotachylite derived from a part of the breccia (or of a larger precursor rock or another area of the source crater) richer in highland materials than the bulk meteorite and the part represented by the analyzed subsamples (see Figs. 7 and 8).

The bulk composition of QUE 94281 is very similar to that of Y-793274 (Table 1); but with ~13 wt% FeO and 17 wt% Al_2O_3, QUE 94281 is less slightly less mafic. (Arai and Warren (1998) report compositions for other subsamples of QUE 94281 that are, on average, more mafic than those we analyzed.) Trace element concentrations are generally similar (Table 2) but differ in detail (Fig. 9). The Sc concentration of Y-793274 (32.5 ppm) exceeds that of QUE 94281 (28.4 ppm) in the samples we analyzed. Although this difference appears not to be significant given the variability among subsamples (~±5 ppm), we note that pyroxene concentrates Sc, thus this difference, if applicable to the entire meteorite, would imply a slightly greater proportion of mafic constituents in Y-793274 (see, however, Arai and Warren, 1998). On the other hand, the concentration of Eu, which is compatible in plagioclase, is not enriched in QUE 94281 relative to Y-793274. Subsamples of these two meteorites reveal two different trends on a plot of Sc *vs.* Eu (Fig. 9c); these trends also occur for Sc *vs.* Na_2O and Sr, which suggests that this is not an artifact of interlaboratory bias in the analyses. The divergence of the two trends in the less mafic subsamples represents a difference in plagioclase of feldspathic components of the two meteorites. The concentrations of incompatible trace elements (ITE) are in most cases slightly greater in QUE 94281 (Fig. 9c,d), and the La:Yb ratio of QUE 94281 (2.76) exceeds slightly that of Y-793274 (2.56), which is consistent with a greater proportion of mafic materials (low La/Yb) in Y-793274.

Concentrations of siderophile elements are significantly higher in QUE 94281 than Y-793274, for example; concentrations of Ni are higher by about a factor of three and concentrations of Ir by a factor of two. As with other lunar meteorites (*e.g.*, Korotev *et al.*, 1996), concentrations and ratios of siderophile elements (Ni, Co, Ir, and Au) in QUE 94281 are consistent with a component of chondritic meteorite that varies in abundance among the subsamples

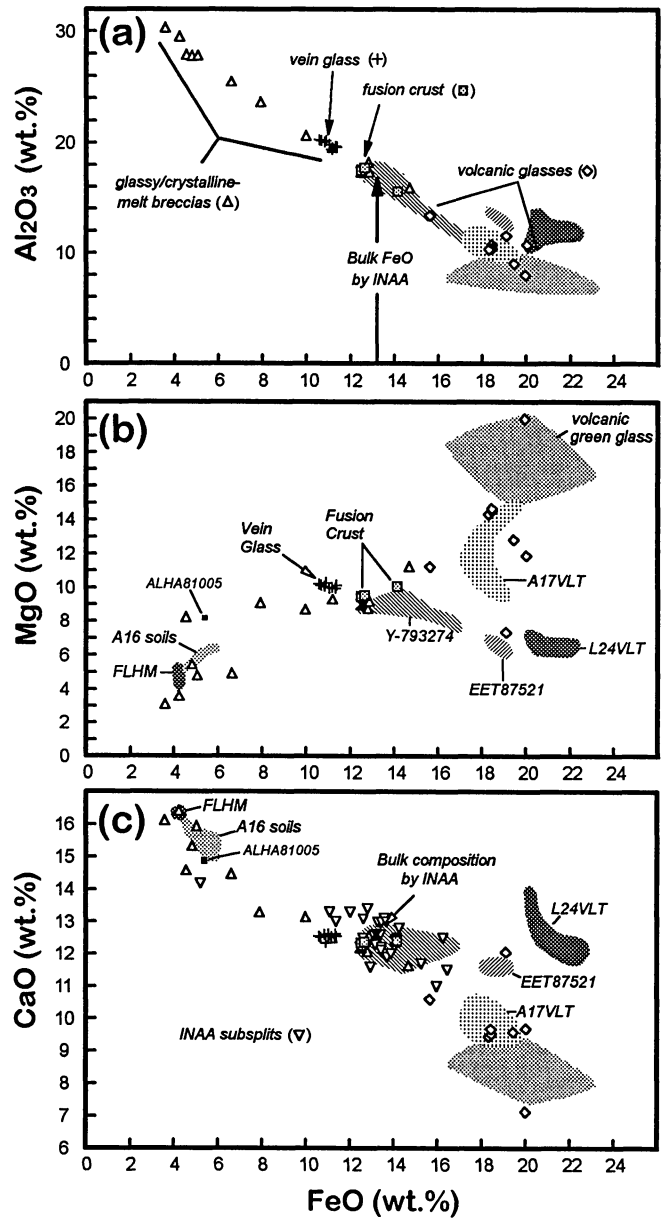

FIG. 7. Concentrations of FeO *vs.* major-element oxides (a) Al_2O_3, (b) MgO, and (c) CaO in QUE 94281 compared to compositions of other highland and mare materials. Symbols represent analyses of QUE 94281: fusion crust (squares), lithic clasts (upright triangles), and volcanic-glass clasts (diamonds) analyzed by EMP, and breccia subsamples analyzed by INA (inverted triangles, (c) only). For the glass clasts labeled as such, a volcanic origin is inferred from their major element compositions. In (a–c), ranges of compositions are shown for subsamples of the two lunar meteorites most similar to QUE 94281: Y-793274 and EET 87521 (Fukuoka, 1990; Lindstrom *et al.*, 1991b; Koeberl *et al.*, 1991; Warren and Kallemeyn, 1991; and Yanai and Kojima, 1991). Ranges are also shown for Apollo green volcanic glass (Taylor *et al.*, 1991; Steele *et al.*, 1992), Apollo 17 VLT glasses and rocks (Vaniman and Papike, 1977; Wentworth *et al.*, 1979; Lindstrom *et al.*, 1994; Jolliff *et al.*, 1996b), and Luna 24 VLT lithologies (Taylor *et al.*, 1991). In (b) and (c), ranges are shown for three feldspathic lunar-highland meteorites (FLHM): Y-86032 (Koeberl *et al.*, 1989), MAC 88105 (Jolliff *et al.*, 1991), and QUE 93069 (Korotev *et al.*, 1996); and for Apollo 16 soils (Korotev, 1981). Lunar meteorite ALHA81005 is distinctly more magnesian than other lunar-highland meteorites (Korotev *et al.*, 1983) and is shown separately in (b) and (c).

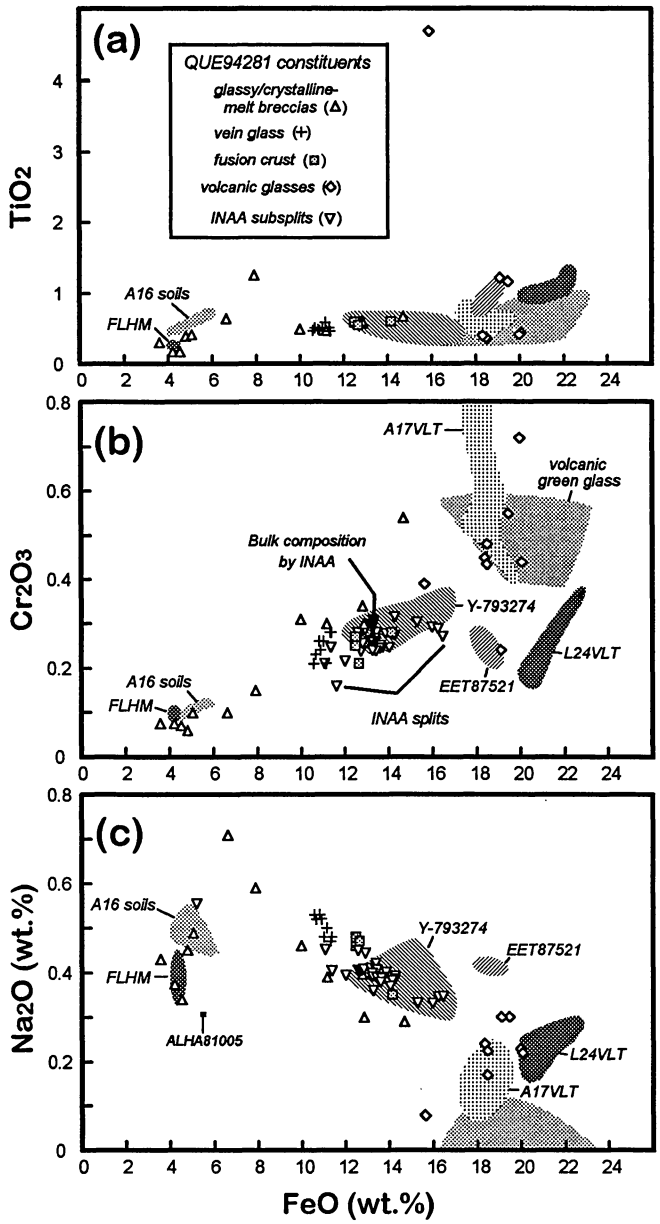

FIG. 8. Concentrations of FeO *vs.* minor element oxides (a) TiO_2, (b) Cr_2O_3, and (c) Na_2O in QUE 94281 compared to compositions of other highland and mare materials. Symbols represent analyses of QUE 94281: fusion crust (squares), lithic clasts (upright triangles), and volcanic-glass clasts (diamonds) analyzed by EMP, and breccia subsamples analyzed by INA (inverted triangles, (b) and (c) only). Shown for comparison are compositions of lunar meteorites Y-793274, EET 87521, feldspathic lunar-highland meteorites (FLHM), Apollo 16 soils, and ALHA81005 ((c) only); and Apollo green volcanic glass, Apollo 17 VLT, and Luna 24 VLT. Symbols and references for data other than QUE 94281 are the same as for Fig. 7.

(Fig. 10). On average, siderophile element concentrations correspond to ~1.6% volatile free, CI-chondrite component. This component probably derives largely from micrometeorites that formed the regolith from which the breccia was formed. Average concentrations of siderophile elements in QUE 94281 are at the high end of the range observed in lunar meteorites and comparable only to Calcalong Creek (Hill *et al.*, 1991) and QUE 93069, which suggests that QUE 94281 formed from near-surface regolith (Korotev *et al.*, 1996). The lower siderophile-element concentrations of Y-793274 (Fig. 10) imply that it was derived from deeper within the regolith or that the components of the meteorite were not exposed at the surface for as long a time.

Mafic, presumably volcanic glass debris is present in QUE 94281, as it is in Y-793274 (see also Warren and Arai, 1997). Most of the small, elliptical glass clasts or fragments that we analyzed in QUE 94281,10 have low-Ti or VLT basaltic compositions ($TiO_2 \leq$ 1.2 wt%, Table 3 and Fig. 8a), as found by Warren and Arai (1997) for a larger sampling of glass spherules. Most have very low TiO_2 concentrations (~0.4 wt%) and are relatively ferroan, having a low *Mg′* value, which is similar to Apollo 17 VLT compositions (*e.g.*, Wentworth *et al.*, 1979; Lindstrom *et al.*, 1994) (Fig. 7b). Glasses with low TiO_2 (1.2 wt%) are presumably part of another group but are not as abundant as the VLT glasses (Warren and Arai, 1997). Others that we analyzed include one with an ultramafic composition (MgO ~ 20 wt%) and one of medium TiO_2 concentration (4.8 wt%). An average composition for all the analyzed mafic glasses is given in Table 1; average compositions of the VLT and LT glass groups are given in Table 3.

The clast population of QUE 94281 includes a substantial proportion of glassy to cryptocrystalline, relatively feldspathic (*i.e.*, nonmare) impact-melt breccias (Table 3). These are the main highland clast constituents. Alumina concentrations range from 17 to 30 wt% and FeO, 4–14 wt% (Fig. 7a and Table 3). Of the most aluminous ones (Al_2O_3 > 27 wt%), most have relatively ferroan matrix compositions (*Mg′* ~ 58–65) and incompatible element concentrations (Ti, K, P) as low or lower than the highly aluminous Apollo 16 group 3 and 4 melt breccias (Korotev, 1994). Of those clasts analyzed by EMPA, which included the largest ones, only one had an *Mg′* value substantially higher (*Mg′* ~ 76, Table 3) than the ferroan group. The compositions of the more ferroan, aluminous group suggest a relatively ferroan, noritic-anorthosite precursor. The magnesian impact-melt clast (Table 3, col. 3) has a normative composition of troctolitic anorthosite, similar to Apollo 16 magnesian granulitic breccias (Korotev, 1997).

The less aluminous impact-melt clasts (Al_2O_3 ~ 17–25 wt%) reflect relatively mafic precursors, but all have low K_2O concentrations (<0.2 wt%), unlike most Apollo crystalline melt-breccia groups (Taylor *et al.*, 1991). These differ from the "KREEP-poor impact melts" from Apollo 15 reported by Lindstrom *et al.* (1990) by their lower TiO_2 concentrations and *Mg′* values. The melt breccias in QUE 94281, however, are similar in composition to clasts observed in feldspathic lunar meteorites (*e.g.*, MAC 88105; Jolliff *et al.*, 1991). These have normative compositions of anorthositic norite to norite, are relatively ferroan (*Mg′* ~ 54–62), and have low TiO_2 concentrations (0.5–0.6 wt%). Only one of the relatively mafic melt-breccia clasts that we analyzed in QUE 94281 is somewhat more magnesian (*Mg′* = 67) and has TiO_2 = 1.3 wt%, which is similar to melt breccias of some of the Apollo 16 groups (*e.g.*, 66095; Taylor *et al.*, 1991; Korotev, 1994).

Trace element compositions are similar for most of the breccia subsamples analyzed by INAA, and they cluster about the mean composition (Fig. 9; Tables 2 and A1). This similarity is consistent with the observation that most of the breccia subsamples are fine-grained and, with the exception of subsample 35A, contain no large clasts. Among those that are the least mafic, judging by Sc concentrations (*e.g.*, Fig. 9 a,b), the concentrations of incompatible trace elements are low, ranging from ~0.04–0.07× those of high-K KREEP (Warren, 1989). This range is higher than in other lunar

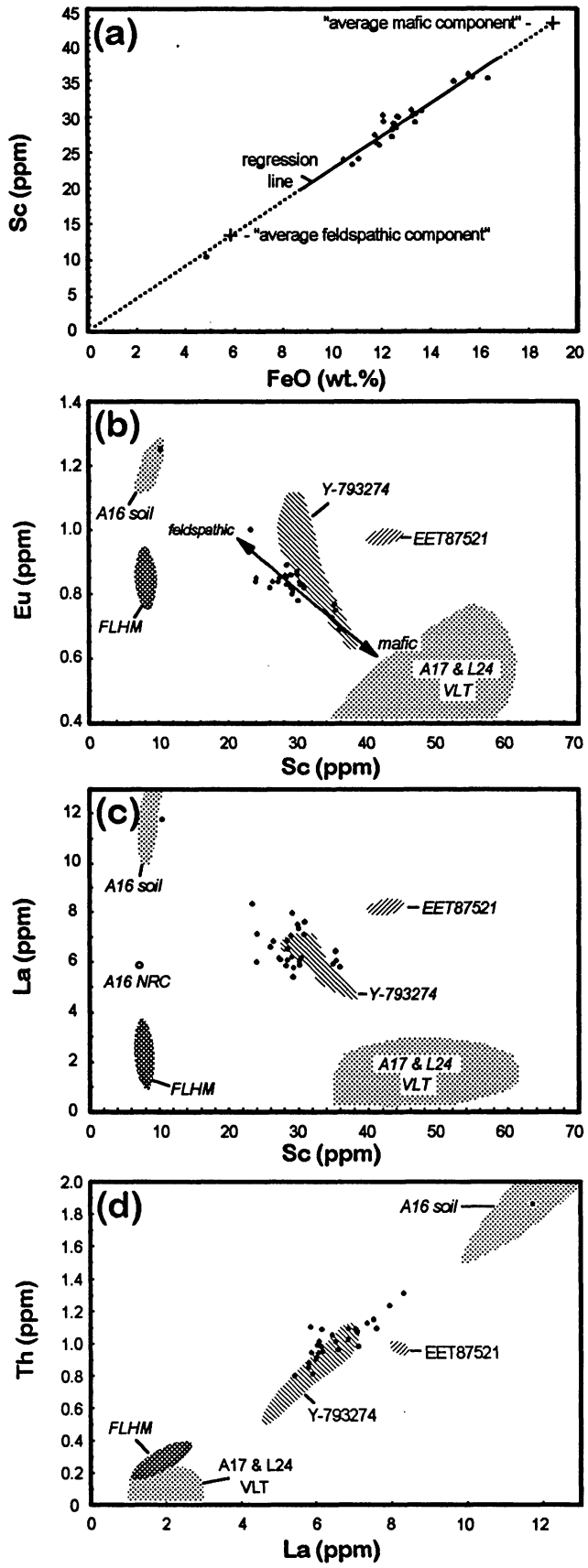

FIG. 9. (Left) Trace element concentrations of QUE 94281 compared (in b–d) to Apollo 16 soil, feldspathic lunar-highland meteorites (FLHM), lunar meteorites Y-793274, EET 87521, and other VLT lithologies. (a) Correlation between Sc and FeO in subsamples of QUE 94281 (corrected for small meteoritic Fe component). The "average mafic component" of QUE 94281 refers to the average composition of all mafic, presumably mare-related materials in the meteorite and is taken to have an FeO concentration of 19 wt%. The extrapolated Sc concentration based on the regression is 43 ppm. The "average feldspathic component" of QUE 94281 refers to the average composition of all highland materials in the meteorite and is taken to have an FeO concentration of 5.9 wt%; the extrapolated Sc concentration based on the regression is 13 ppm. (b) Sc *vs.* Eu; data points shown only for QUE 94281. Fields shown for others are based on data referenced in the Fig. 7 caption. Scandium and Eu are inversely correlated similarly to Sc-Na_2O and Sc-Sr. The more mafic subsamples have the lowest Eu concentrations and highest Sc concentrations, and the most feldspathic subsamples have the highest Eu concentrations and lowest Sc concentrations, which is consistent with partitioning of these two elements between pyroxene and plagioclase. Elephant Moraine 87521 lies well off the trend for QUE 94281 subsamples, and Y-793274 appears to have more Eu-rich highland components than QUE 94281. The range of Eu concentrations for subsamples that have <30 ppm Sc reflects a range of Eu concentrations in highland constituents of QUE 94281. Ranges of compositions are shown for Apollo 16 soils and feldspathic lunar-highland meteorites for comparison (see Fig. 7 caption). (c) Sc *vs.* La, in which La represents a typical incompatible trace element (ITE). The correlation for QUE 94281 subsamples is poorer than in (b) and reflects variability in the ITE enrichment of highland materials in QUE 94281. Other highland compositions shown for comparison. Soil from North Ray Crater at Apollo 16 differs from other Apollo 16 soils and is shown separately. On the mafic (Sc-rich) side, EET 87521 lies away from the cluster of QUE 94281 data, but the range of Y-793274 data differs from QUE 94281 only in having slightly greater Sc and lower La concentrations. (d) La *vs.* Th; both are incompatible trace elements and are fairly well correlated. Although the two most feldspathic subsamples have the highest ITE concentrations, the most mafic subsamples do not necessarily have the lowest ITE concentrations (cf., (c)), reflecting the variability of ITE enrichment in the highland materials. Apollo 16 soils are significantly enriched in ITE relative to QUE 94281 and its inferred highland components, with the exception of clast 35A1 (Table A1); whereas, the feldspathic lunar-highland meteorites have much lower ITE concentrations.

meteorites that consist mainly of highland materials, such as QUE 93069, MAC 88104/5, Y-791197, Y-82192/3, and Y-86032, but less than in Calcalong Creek (Hill *et al.*, 1991) by a factor of three to five. Subsample 35A is enriched in all incompatible trace elements in roughly KREEP-like proportions (Table A1); however, its low FeO concentration (35A1: 5.2 wt%, Table A1) and its appearance (white, granulitic, plagioclase-rich) are not typical of Apollo impact-melt breccias. In thin section, the only highland lithic clast obviously enriched in incompatible elements is the olivine- and whitlockite-bearing feldspathic granulite shown in Fig. 3e. On a plot comparing two incompatible trace elements, analyses of breccia subsamples reveal correlated variations that extrapolate toward the compositions of subsamples 35A and B, which suggests that this or some similar lithology is present as fine-grained clasts or in the matrix of other subsamples of QUE 94281 breccia.

DISCUSSION

Estimating the Compositions of Average Mafic (Mare) and Feldspathic (Highland) Components

From the variability in compositions of subsamples of QUE 94281, we can estimate the average compositions of the mafic and feldspathic components. In this context, "component" refers to the set of constituents that were derived from mare-related volcanic activity or as part of the older, feldspathic highlands. Linear trends on plots such as FeO *vs.* Al_2O_3 and others (Figs. 8 and 9) imply, to a first approximation, binary mixing between the highland and mare components. We can use the trends to extrapolate to the average

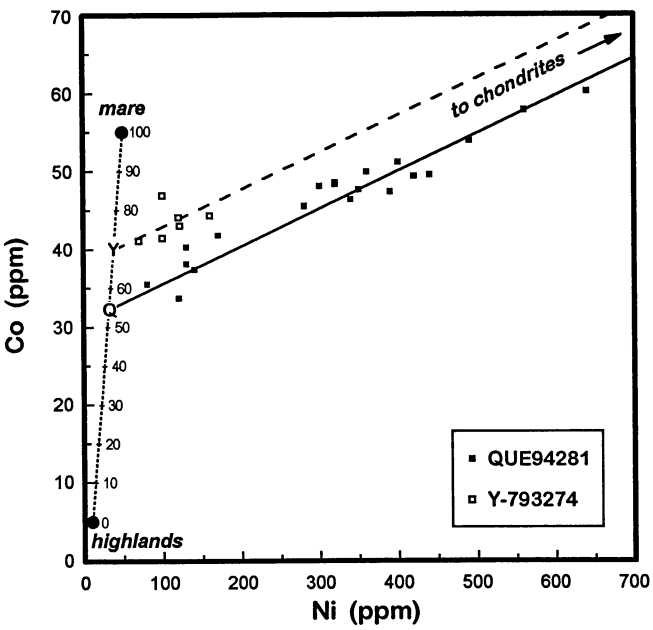

FIG. 10. Cobalt and Ni variation among subsamples of QUE 94281 and Y-793274. For this plot, subsamples of QUE 94281 that are compositionally dissimilar to the average composition are not plotted. Nickel and Co are contributed by three components in the meteorites, a chondritic meteorite component that plots off scale at ~11 000 ppm Ni (assuming CI chondrite) and lunar mare and highland components. The concentrations of Ni and Co in the mare and highland components are not known, but the concentrations plotted here (circles) are consistent with known VLT basalts and feldspathic highland materials free of meteoritic contamination. The solid, diagonal line is a regression line fit to the QUE 94281 data. Extrapolation of the line to 11 000 ppm Ni gives a Co concentration of 561 ppm Co and a Ni/Co ratio of 19.6, that is, well within the range of chondrites. Thus, the distribution of points is, in fact, consistent with mixtures of lunar materials having the concentrations represented by the point Q (*i.e.*, a 54:46 mixture of mare and highland components) and some type of chondritic material. The range of Ni concentrations among the subsamples corresponds to a range of 0.3% to 4.1% volatile free, CI-chondrite component. The dashed line is defined by the chondritic component and the average composition of the six subsamples of Y-793274. The point Y represents the mean, indigenous concentrations of Ni and Co in the lunar components of Y-793274. The Co concentration (~40 ppm) is greater than the corresponding concentration for QUE 94281 (~32 ppm) because Y-793274 has a greater proportion of mare material. Yamato 793274 data are from Fukuoka (1990), Koeberl *et al.* (1991), Lindstrom *et al.* (1991b), and Warren and Kallemeyn (1991).

compositions of the two endmembers. By assuming an average FeO concentration of 19 wt% for the mafic components and 5.9 wt% for the feldspathic components, the concentrations of the other major element oxides can be determined based on the extrapolation of trends for each oxide and FeO. Then, given the bulk composition of the meteorite and mass-balance constraints, we can determine their relative proportions (Warren and Kallemeyn, 1991, applied a similar graphical technique to Y-793274). We estimate the bulk composition of QUE 94281 from that of the fusion crust (EMPA) and the mass-weighted mean composition of all subsamples (INAA, Table 2).

An FeO concentration of 19 wt% is about the same as for other VLT mare basalts that have similar mafic-mineral compositions to those found in QUE 94281 (*e.g.*, Apollo 17 VLT and EET 87521, Fig. 7 and references listed in the caption). To estimate the major element compositions of the average feldspathic and mafic components, we use all subsample (INAA) and constituent (EMPA) compositions having FeO concentrations between 8 and 17 wt%, including magnetic separates of subsample 33 (Table A1). This restriction excludes the highly feldspathic and mafic clasts that would tend to dominate the linear regression. From the regression of these data against FeO and extrapolation to 19 wt%, we estimate the average composition of mafic components to be that given in Table 4 (column 1). This composition is similar to the average composition of mafic glasses (Table 1) but has lower TiO_2, Cr_2O_3, and MgO. By linear regression, the concentration of the trace element Sc, which correlates well with FeO, is 43 ppm at FeO = 19 wt% (Fig. 9a). This is low relative to most mare basalts but in the range found for other lunar volcanic VLT basalts and glasses (Taylor *et al.*, 1991). We have not estimated concentrations of the other trace elements in the mafic component using this method because most do not correlate well with FeO, with the exception of Eu and Sr (see below).

To estimate the average composition of highland components, we assume an FeO concentration equal to the average for nine highland clasts as measured in thin section (5.9 wt%, Table 1). These clasts represent the most prominent, recognizably highland constituents of the breccia. Then, extrapolation of the regressed data to 5.9 wt% yields the composition given in Table 4. From the bulk FeO concentration of the meteorite (represented by the fusion crust (13 wt%), the FeO concentrations of the average mafic and feldspathic endmembers, and mass balance), the mass proportions of mafic and feldspathic components are found to be 54% and 46%, respectively. Even if the average FeO concentration of feldspathic components turned out to be lower, say as low as 4.5 wt%, the proportion of feldspathic components in QUE 94281 would still exceed 40%. On the other hand, the fact that single-mineral clasts and glasses related to mafic components outweigh highland lithic clasts argues against the proportion of highland materials *exceeding* 46%.

Highland Components–The average composition of highland components calculated as described above has an Al_2O_3 concentration of ~26 wt% and is similar to that of the average measured composition of highland clasts based on EMP analyses (Table 1). The average highland composition estimated by the regression method, however, has a significantly higher MgO concentration than the average of clasts measured by EMP analyses, 8 wt% *vs.* 6 wt%. This suggests that there may be a highland component more magnesian than any of the feldspathic clasts we analyzed in the thin section. Likewise, the estimated average MgO concentration of the mafic components is less than that of the analyzed mafic glasses, 11.0 wt% *vs.* 13.4 wt%. This disparity occurs partly because we excluded outliers in the regression analysis and partly because the glass vein, which is included in the regression analysis, has a relatively high MgO concentration compared to measured highland clasts and the fusion crust (Fig. 7b). We found no feldspathic clasts having compositions sufficiently magnesian to have caused the magnesian glass-vein composition; however, olivine and pyroxene grains that have *Mg'* as high as 80 are found among mineral and lithic clasts.

The estimate of average Na_2O concentration of highland components by the regression method also exceeds the average Na_2O of analyzed highland clasts, suggesting, as for MgO, a cryptic or under sampled Na_2O-rich highland component. One of the feldspathic melt-breccia clasts analyzed by EMP has an Na_2O concentration of 0.7 wt%, and several plagioclase grains have Na_2O concentrations >1% and as high as 4% (Table A5, lithic clast 2). Furthermore at the mafic end of the regression, the extrapolated Na_2O concentration compares well to what was expected, based on the average Na_2O concentration of plagioclase clasts (~0.9 wt%, Table A3) and their

TABLE 3. Major element compositions of representative glass and fine-grained lithic clasts in QUE 94281,10.

	Glassy-crystalline Melt Breccias							Mafic Glasses			
	anorthositic			noritic							
	ferroan		magnesian	Al, fer	Al, mag	Maf a	Maf b	VLT	MG	LT	MT
n	3	2	1	1	1	3	2	4	1	2	1
SiO_2	45.1	45.2	42.9	46.7	44.4	46.3	46.4	45.7	44.2	46.8	43.0
TiO_2	0.26	0.41	0.18	0.65	1.27	0.53	0.63	0.40	0.41	1.20	4.78
Al_2O_3	30.1	27.8	27.9	25.5	23.7	19.5	16.7	10.6	8.0	10.3	13.4
Cr_2O_3	0.08	0.08	0.07	0.1	0.15	0.32	0.42	0.45	0.72	0.40	0.39
FeO	3.79	4.92	4.53	6.61	7.90	11.3	13.8	18.8	20.0	19.3	15.6
MnO	0.04	0.05	0.08	0.11	0.07	0.16	0.19	0.23	0.23	0.27	0.22
MgO	3.27	5.18	8.26	4.95	9.09	8.94	10.2	13.9	20.0	10.1	11.3
CaO	16.2	15.6	14.6	14.5	13.3	12.6	12.1	9.60	7.16	10.8	10.6
Na_2O	0.41	0.47	0.34	0.71	0.59	0.42	0.30	0.21	0.23	0.30	0.08
K_2O	0.02	0.07	0.01	0.11	0.11	0.14	0.08	0.01	0.02	0.05	0.01
P_2O_5	nd	nd	nd	nd	0.19	nd	0.05	nd	nd	0.10	<0.02
Sum	99.3	99.9	98.9	99.9	100.6	100.2	100.8	99.9	101.0	99.6	99.3
*Mg'	60.6	65.3	76.5	57.2	67.2	58.5	57.0	56.8	64.2	48.3	56.2

*Mg' = molar MgO/(MgO + FeO) × 100. Oxides given in weight percent, determined by EMPA. Abbreviations: Al, fer = aluminous, ferroan; Al, mag = aluminous, magnesian; Maf a = mafic group a; Maf b = mafic group b; VLT = very-low-Ti, MG = magnesian; LT = low-Ti; MT = medium-Ti.; nd = not determined.

proportion (~30%) associated with the mafic component. By this reasoning, the Na_2O concentration of the mafic component should be 0.26–0.28 wt%, which is consistent with the estimate based on regression. This range is also consistent with correlated variations between FeO-Eu (or Sc-Eu, Fig. 9b) and Eu-Na_2O for subsamples analyzed by INA, which indicate an Na_2O concentration of ~0.26–0.28 wt% at an Eu concentration of 0.58 ppm, corresponding to 19 wt% FeO.

A similar calculation for MgO based on MgO concentrations of pyroxene and olivine clasts (yielding an estimate of 10.8 wt% average for mafic components) is consistent with the regression-based estimate of average MgO concentration of mafic components of 11.0 wt% and, thus, supports the regression estimate for the highland components (8 wt%). However, MgO concentrations of pyroxene and olivine clasts span a broad range, making this calculation less convincing than that for Na_2O.

The average composition of the highland components in QUE 94281 estimated as described above is similar to the bulk compositions of ALHA81005, Y-82192/3, and Y-791197. Allan Hills A81005, which is more magnesian (*i.e.*, higher Mg/Fe) than the others (Laul *et al.*, 1983), is similar to our regression estimate shown in Table 4. The more ferroan average measured composition of feldspathic clasts in QUE 94281 is similar to the bulk compositions of Y-82192/3, Y-791197 (see Koeberl *et al.*, 1989), and to average Apollo 16 soil (Korotev, 1981). The lunar meteorites Y-82192/3 and Y-791197 contain a small mare component, and Apollo 16 soils contain a mafic impact-melt-breccia component (see Korotev, 1997). The highly feldspathic lunar-highland meteorites, QUE 93069/QUE 94269, MAC 88104/5, and Y-86032 have lower FeO concentrations (~4–5 wt%), more like the prebasin compositions of Korotev (1996b) based on Apollo 16 ancient regolith breccias and feldspathic fragmental breccias. These more feldspathic compositions, similar to those of some of the individual clasts in QUE 94281 (see below), may be representative of large parts of the lunar-highland surface, especially away from the large, nearside basins. Clementine remote sensing also supports lower FeO concentrations (~4 wt%) over much of the farside highland surface (Lucey *et al.*, 1995).

The concentrations of incompatible trace elements in QUE 94281 (and, on average, in its highland components) are greater than those of the other lunar-highland meteorites (except Calcalong Creek), but they are lower than in highland soils from the Apollo 16 site (Fig. 9c,d). The low ITE concentrations indicate that most of the clasts of impact-melt breccia in QUE 94281 are incompatible element poor and derived from impacts that excavated mainly KREEP-poor, feldspathic upper crust; whereas, the mafic impact-melt component of Apollo 16 soils is basin derived (Korotev, 1997). Several of the impact-melt clasts in QUE 94281 have compositions similar to the most feldspathic lunar highland meteorites (Figs. 7 and 8), including low Mg', low TiO_2, and low Na_2O, which suggests that a source for these constituents was not far away. In the case of QUE 94281 and Y-793274, this poses something of a quandary: the source area must have been near or at the boundary between a mare and a highland region but also near an area of feldspathic highlands uncontaminated by ITE-rich, mafic impact-melt lithologies. Perhaps this means that the basin containing the mare volcanic rocks did not produce and eject particularly mafic and ITE-rich impact melts.

Mafic Components–The mafic components in QUE 94281 have, on average, a very low TiO_2 concentration (~0.8 wt%). Overall, the mafic components as a group are similar in composition to EET 87521 and to the inferred mafic component of Y-793274. In fact, using the average compositions of mafic and feldspathic components in QUE 94281 (Table 4), the bulk composition of Y-793274 (Table 1) is closely matched with ~62% of the average mafic component and 38% of the average feldspathic component. This is in good agreement with Warren and Kallemeyn (1991), who estimated two-thirds mare components and one-third highland components for Y-793274. A greater proportion of mare components in Y-793274 compared to QUE 94281 is also consistent with lower La/Yb in Y-793274. The composition of EET 87521, however, cannot be matched using a binary mixture of the average highland and mare components of QUE 94281 because EET 87521 is too ferroan and its concentrations of TiO_2 and Al_2O_3 are too high. Furthermore, the concentrations of most incompatible trace elements in EET 87521 are high relative to both QUE 94281 and Y-793274 (Fig. 9c,d). The

TABLE 4. Major element compositions of feldspathic and mafic components of QUE 94281.

	Estimated Components[1]			EET 87521[2]	Model Derivative Magmas[3]			
	Mafic	Feld-spathic	Crystalline VLT	Bulk, Lit Avg.	Fractional Crystallization, 3 kb Starting	24%	35%	45%
SiO_2	47.0	44.9	47.0	47.9	43.8	45.2	46.6	47.3
TiO_2	0.83	0.31	0.80	0.97	0.41	0.51	0.56	0.65
Al_2O_3	10.2	25.6	10.2	13.2	7.9	9.7	10.6	12.3
Cr_2O_3	0.37	0.13	0.36	0.24	0.71	0.43	0.11	0.12
FeO	19.0	5.89	19.0	18.8	19.8	20.8	21.0	20.5
MnO	0.28	0.08	0.28	0.24	0.23	0.24	0.24	0.24
MgO	11.0	8.1	10.8	6.79	19.8	13.9	10.3	6.90
CaO	10.9	14.3	11.0	11.6	7.1	8.9	10.2	11.6
Na_2O	0.26	0.68	0.26	0.42	0.23	0.29	0.33	0.39
K_2O	0.05	0.10	0.05	0.06	0.02	0.03	0.03	0.04
P_2O_5	0.06	0.07	0.06	–	0.02	0.03	0.03	0.04
Mg'	51.2	71.0	50.8	39.2	64.2	54.2	46.5	37.5

Mg' = molar MgO/(MgO + FeO) × 100; oxides given in weight percent. [1]Feldspathic (highland) and mafic (mare) components estimated by regression of data for subsamples as described in text. Proportions are mafic/feldspathic: 54/46 (wt%). The values in the first column are normalized so that the sum of oxides = 100% (raw estimate sums to 101%). Crystalline VLT component calculated assuming the mafic component = 92% crystalline VLT and 8% mafic glass (Table 1); proportions are based on image analysis. [2]Composition of EET 87521 is an average of two compositions given by Warren and Kallemeyn (1991). [3]Model derivative magma compositions calculated using mafic glass "MG" (Table 3) as starting composition (reproduced here, normalized to 100%). Compare composition at 24% to "VLT" mafic glass (Table 3); compare 35% to "crystalline VLT" (this table); and 45% to EET 87521 (this table). Derivative compositions calculated mainly by subtraction of olivine of relevant *Mg'* plus minor Cr-spinel; percent crystallization given as mol%. Calculations made using fractional crystallization program of Longhi (*e.g.*, 1982, 1986).

average TiO_2 concentration of mafic components in QUE 94281 is significantly less than those of the other two basaltic meteorites Y-793169 and A-881757, which have bulk TiO_2 concentrations of ~2–2.5 wt% (Jolliff *et al.*, 1993).

The Crystalline VLT Component

From the relative proportions of coarse, single-mineral clasts and glass clasts, we have estimated the relative proportions of the crystalline VLT component and mafic glasses. Using image analysis of a digital backscattered-electron image (same as used to make Fig. 1), the proportion of coarse mineral clasts is ~19.1% and mafic glasses, 1.6% (vol%). Thus, the mafic components include ~8% mafic glass and 92% of a crystalline VLT component, and the composition of the latter can be calculated (Table 4). This composition is very similar to the average composition of mafic components and has TiO_2 <1 wt%.

The coarse, crystalline clasts of pyroxene, plagioclase, and olivine appear to be derived largely from a single parent rock formation (*i.e.*, the crystalline VLT component). Of the large pyroxene clasts that we analyzed in QUE 94281, nearly all have compositions that are consistent with a single fractionation trend (Fig. 5). These range from low-Ca pyroxene with an *Mg'* value of ~70 to ferroaugite with *Mg'* ~ 20 and hedenbergite with *Mg'* <5 (Table A2). Separate grains of hedenbergite, fayalite and cristobalite, as well as eutectoid intergrowths of these three minerals plus K-feldspar almost certainly are cogenetic with the main-trend pyroxenes because pyroxene compositions cover the range of Fe enrichment coupled with Ti enrichment and Cr depletion (Fig. 5) leading to hedenbergite. Also, several of the coarse pyroxenes are intergrown with plagioclase grains (see Table A3). The proportion of coarse plagioclase clasts relative to coarse pyroxene in QUE 94281 (based on image analysis of QUE 94281,10, discussed above) is close to what would be expected (slightly less) if they were all derived from the same parent rock formation. In other words, from the composition of the crystalline VLT component (Table 4), we calculate a pyroxene to plagioclase volume ratio of ~1.6, and the observed ratio of coarse pyroxene to plagioclase clasts is ~1.8. Thus, we conclude that virtually all of the coarse plagioclase single-mineral clasts are related to the coarse pyroxene and that there is predominantly a single crystalline mafic component (or parent rock formation) represented by the coarse mineral clasts in QUE 94281. Because of the coarse grain size, including the development of relatively coarse-grained, late-stage hedenbergite, fayalite, and cristobalite, we refer to this as the QUE 94281 VLT-gabbro component.

The VLT-Gabbro Composition Compared to Other VLT Compositions

The composition of the QUE 94281 VLT gabbro, derived as described above, is similar to that of the QUE 94281 VLT volcanic glasses (Table 3), except that it is slightly poorer in MgO and Cr_2O_3 and richer in TiO_2, CaO, Na_2O, and K_2O. These differences are qualitatively consistent with the VLT gabbro being a fractionate of the same parent magma represented by the VLT glasses (discussed in more detail in the next section). In the following discussion, we take the QUE 94281 VLT component to include both the VLT gabbro and VLT volcanic glasses; these are compared to EET 87521, Y-793274, and Apollo 17 and Luna 24 VLT lithologies.

The composition of the QUE 94281 VLT component differs from that of lunar meteorite EET 87521, which has little or no highland component (Warren and Kallemeyn, 1991); however, the differences in major elements suggest (at least to a first approximation) that EET 87521 could be a derivative of a similar parent magma. The composition of EET 87521 is substantially more ferroan, having an *Mg'* value of ~39 compared to ~51 for the QUE 94281 VLT component (Table 4). This is consistent with the compositions of pyroxenes, which are, as a group, more Fe-rich in EET 87521 (Yanai and Kojima, 1991). Furthermore, EET 87521 has higher con-

centrations of TiO_2, Na_2O, Al_2O_3, and SiO_2, which is qualitatively consistent with its being more fractionated or "evolved" than the QUE 94281 VLT-gabbro component. Quantitatively, however, the concentration of TiO_2 exceeds the calculated concentration derived by fractional crystallization (see discussion below and model compositions, Table 4). Trace element concentrations also separate EET 87521 from QUE 94281 (Fig. 9) and preclude any direct petrogenetic relationship.

Similarities in bulk and constituent compositions between QUE 94281 and Y-793274 (Table 2, Figs. 7, 8) and petrographic similarities suggest that the VLT components of the two meteorites represent similar protoliths. Compositions of mafic subsamples of both meteorites overlap for most elements; however, there are differences in variations of MgO and Cr_2O_3 that are difficult to explain. One trend among subsamples of Y-793274 on the plot of MgO *vs.* FeO (Fig. 7b) extrapolates toward the bulk composition of EET 87521; taken alone, this might indicate a relationship between the dominant mafic component of Y-793274 and EET 87521. However, the trend for mafic subsamples of Y-793274 for Cr_2O_3 *vs.* FeO does not extrapolate to EET 87521 (Fig. 8b). On the other hand, for QUE 94281, the Cr_2O_3 concentrations of several whole-rock subsamples analyzed by INAA, including the pyroxene-rich (Sc concentration = 36 ppm) magnetic separate, extrapolate toward the relatively Cr-poor composition of EET 87521. Perhaps, these subsamples are enriched preferentially in the more Fe-rich pyroxenes, which have lower Cr_2O_3 concentrations than the more magnesian pyroxenes (Table A2). If so, this may explain the apparent discrepancy between the lower concentration of Cr_2O_3 in the VLT gabbro that could be inferred from Fig. 8b (<0.3 wt%) and that obtained by the mass-balance method described above (0.36–0.37, Table 4).

Bulk lithophile trace element concentrations of QUE 94281 and Y-793274 are, to a first approximation, similar, differing slightly in the levels of trace elements associated with mafic *vs.* feldspathic components, as discussed above. On closer inspection, however, the concentrations of some elements in *subsamples* of the two meteorites define slightly different trends. On a plot of Eu *vs.* Sc (Fig. 9b), which separates feldspathic from mafic components, the mafic components of the two meteorites appear to be similar, but highland components define two different trends, with subsamples of Y-793274 extending to higher Eu concentrations. A plot of La *vs.* Sc, however, suggests a difference in the mafic components as well (Fig. 9c). Relative to variations found among highland materials of Apollo soils, these variations are small and do not necessarily require different source regoliths for the two meteorites, but they do argue against the two meteorites having been ejected from the Moon as portions of the same rock.

The VLT lithologies from Apollo 17 and Luna 24 differ significantly from those of QUE 94281 and Y-793274. Those from Apollo 17 include a variety of textures ranging from volcanic glass to crystalline, but none have been found that have similar coarsely crystalline and exsolved pyroxene. Several of the QUE 94281 glasses have compositions that overlap the range for Apollo 17 VLT lithologies; however, no individual members of these two suites have compositions that are similar for all elements. Also, the Apollo 17 group includes members that have higher Cr_2O_3 and lower Na_2O concentrations than most of those from QUE 94281 (Fig. 8). The Luna 24 VLT basalts are distinctly more Fe-rich, and the extrapolation of compositional trends for subsamples of QUE 94281 and Y-793274 shown in Figs. 7 and 8 preclude any simple relationship to the Luna 24 VLT compositions.

Relationship of QUE 94281 Volcanic Glasses to VLT Gabbro

Given an estimate of the composition of the QUE 94281 VLT gabbro, we consider whether it might be related to any of the QUE 94281 volcanic glass compositions. One of the volcanic glasses is ultramafic (Table 3; "MG") and appears to be a candidate for a parent melt to the suite of VLT components (glasses and gabbro) in QUE 94281. By fractionation (subtraction) of olivine and a minor amount of Cr-spinel at depth (modeled using the fractional crystallization program of John Longhi, *e.g.,* Longhi, 1982), the major element composition of the VLT gabbro is closely matched at ~35% crystallization, and the average major element composition of the relatively ferroan VLT glasses (Table 3) is fairly closely matched at ~24% crystallization (Fig. 11). Thus, both the VLT-gabbro component and the VLT volcanic glasses in QUE 94281 may be petrogenetically related. Because QUE 94281 is a regolith breccia containing a variety of materials that were present at the lunar impact site, a search within other subsamples of this meteorite may reveal additional mafic and ultramafic glass compositions that can be used to test the tentative relationships we suggest above.

As discussed above, EET 87521 appears to have a different crystalline VLT component from that of QUE 94281. In EET 87521, pyroxene compositions are as a group more Fe rich, and concentrations of incompatible trace elements (Table 2) and Ti (Table 4) are higher, which indicate that it is more evolved. These features and the slightly more aluminous nature of EET 87521 are reflected by the location of its bulk composition on the silica-olivine-anorthite pseudoternary phase diagram (Fig. 11) where the bulk composition plots slightly above and to the right of the peritectic point. Given

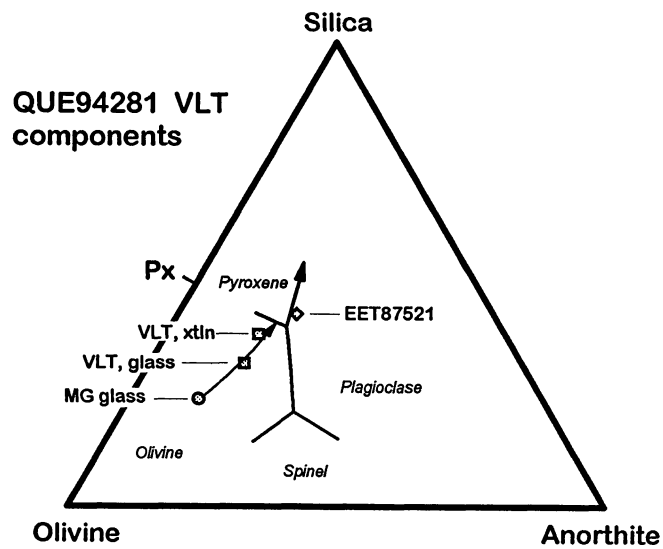

FIG. 11. Silica-olivine-anorthite pseudoternary phase diagram showing QUE 94281 VLT mafic components in relation to melt compositions derived by fractional crystallization of the composition of "MG glass" (Table 3). Phase boundaries in the vicinity of the peritectic point were estimated using the fractional crystallization model of Longhi (1982), for P = 3 kb. Starting with a melt of the composition of "MG glass," olivine crystallization drives the instantaneous residual liquid composition to the pyroxene-olivine cotectic at ~40% crystallization. The average composition of VLT glasses that we measured in QUE 94281 (Table 3) lies along the olivine subtraction line at ~24% crystallization and the composition of the VLT crystalline component lies at ~35% crystallization. The derivative melt composition reaches the peritectic point after ~46% crystallization and plagioclase joins the crystallizing assemblage. The composition of EET 87521, for comparison, plots slightly to the right of the pyroxene-plagioclase cotectic and toward the silica apex, in the direction of melt evolution during fractional crystallization.

the uncertainties associated with our estimate of the composition of mafic components in QUE 94281, it seems possible that the precursor of EET 87521 and the QUE 94281 VLT gabbro could be petrogenetically related. Although such a relationship is qualitatively consistent with trace element differences, we have not modelled trace element evolution rigorously because of uncertainties in their concentrations in the VLT components of QUE 94281. Analyses made by secondary-ion mass spectrometry (SIMS) or microdrilling INAA would allow more detailed modelling and are suggested for future work.

The occurrence in QUE 94281 of a predominant coarse-grained mafic or "mare" component suggests derivation from a single, buried rock formation ("mare gabbro"). The presence of abundant VLT glass indicates proximity to a source of related pyroclastic glass. Fine-grained mare components and constructional particles (*e.g.,* mafic glassy-matrix breccias) are rare to absent among the clasts, suggesting that if the precursor of the meteorite was a mare regolith, it was immature. One possible scenario is that the coarse-grained crystalline VLT gabbro was derived from a hypabyssal intrusive setting, overlain by only thin basalt flows and pyroclastic deposits. In that case, the substantial proportion of highland components indicates that the source was near a mare-highland contact, as advocated by Warren (1994) for Y-793274. At the *Apollo 17* landing site, soils at two of the rover stops in basaltic regolith of the central valley, LRV-3 and LRV-9, have ~55% basalt + pyroclastic glass and 45% highland constituents (Korotev and Kremser, 1992). Perhaps the source was located in a cryptomare (Head *et al.*, 1993) region where an older volcanic surface was covered by a later veneer of highland impact ejecta or mass-wasted debris.

CONCLUSIONS

Lunar meteorite QUE 94281 is a well-lithified, glassy-matrix, clast-rich regolith breccia. Based on our subsamples, the meteorite comprises ~54% mafic or "mare" components and 46% feldspathic or "highland" components. The mafic constituents consist mainly of coarse-grained mineral clasts and mafic volcanic glass fragments, mostly of VLT composition; fine-grained basaltic lithic clasts are rare. Highland constituents include abundant clasts of glassy to cryptocrystalline, incompatible-element-poor feldspathic melt breccias, ranging from 17 to 30 wt% Al_2O_3, and other less common highland lithologies such as granulite and feldspathic impact-melt rocks.

The coarsely crystalline mineral clasts include pyroxenes that contain fine exsolution lamellae and whose compositions are similar to those of known VLT basalts, as well as relatively coarse hedenbergite, fayalite, and cristobalite. Pyroxene compositions and exsolution features indicate a slow-cooling crystallization trend; this trend, coupled with an apparent petrogenetic relationship between nearly all coarse single-mineral clasts in QUE 94281, suggests a VLT-gabbro precursor. An estimate of the composition of this component suggests that it may be cogenetic with some of the volcanic glasses in QUE 94281, related by different amounts of olivine fractionation of a parent magma with a composition like that of a magnesian, picritic glass, also found in QUE 94281.

The regolith represented by this breccia is unlike the mare regoliths sampled at the Apollo sites. It is dominated by coarsely crystalline and presumably immature mafic constituents but contains a substantial proportion of highland materials with, on average, a higher FeO concentration than thought to be typical of much of the farside highlands. The presence of highly feldspathic and ITE-poor impact-melt clasts reflects a nearby highland source that was uncontaminated by mafic melt breccias of the kind sampled by Apollo missions and presumably of basin origin. Perhaps the source regolith for this meteorite formed not in a region of widespread basalt flows, as in a basin-filling mare, but instead formed in a region of localized, near-surface intrusive and volcanic activity or in an area of cryptomare, now covered by a veneer of highland deposits.

The compositions and lithologies of QUE 94281 permit source-crater pairing with Y-793274. Differences in lithophile-element compositions between QUE 94281 and Y-793274 are consistent with the difference in proportions of highland and mare components. Differences in siderophile element compositions are consistent with a higher proportion of extralunar meteoritic material in QUE 94281 and, thus, a greater amount of surface exposure. Although the composition of QUE 94281 differs significantly from that of EET 87521, petrographic and major element compositional similarities between EET 87521 and the VLT-gabbro component of QUE 94281 suggest that they could result from different amounts of fractionation of similar VLT parent magmas. However, differences in minor and trace element compositions preclude a direct relationship between EET 87521 and the VLT-gabbro component of QUE 94281.

Acknowledgments–Funding for this work was provided primarily by NASA grant NAGW-3343 and NAG5-4172 to L. A. Haskin. We thank Dan Kremser for assistance with the JEOL 733. We thank the Meteorite Working Group for making samples of QUE 94281 available to us. We have benefited from discussions about QUE 94281 and other lunar meteorites with our colleagues who share an interest in these important samples, especially Paul Warren and Marilyn Lindstrom. We thank Paul Warren for providing us a preprint of Arai and Warren (1998). Thought-provoking reviews from A. Basu and G. Kurat helped to improve the manuscript and are appreciated.

Editorial handling: U. Krähenbühl

REFERENCES

ARAI T. AND WARREN P. H. (1998) Lunar meteorite QUE 94281: Glass compositions and other evidence for launch pairing with Yamato 793274. *Meteorit. Planet. Sci.* **33,** in press.

ARAI T., WARREN P. H. AND KALLEMEYN G. W. (1996) Lunar meteorite QUE 94281: A possible pair of Y793274 and/or EET87521 (abstract). *Lunar Planet. Sci.* **27,** 33–34.

ARMSTRONG J. T. (1988) Quantitative analysis of silicate and oxide minerals: Comparison of Monte-Carlo, ZAF, and phi-rho-Z procedures. *Microbeam Analysis,* 239–246.

BISCHOFF A. AND WEBER D. (1997) Dar Al Gani 262: The first lunar meteorite from the Sahara (abstract). *Meteorit. Planet Sci.* **32 (Suppl.),** A13–A14.

DELANEY J. S. (1989) Lunar basalt breccia identified among Antarctic meteorites. *Nature* **342,** 889–890.

DREIBUS G., SPETTEL B., WLOTZKA F., JOCHUM K. P., SCHULTZ L., WEBER H. W. AND WÄNKE H. (1996) Chemistry, petrology, and noble gases of basaltic lunar meteorite QUE 94281 (abstract). *Meteorit. Planet. Sci.* **31 (Suppl.),** A38.

EUGSTER O. AND POLNAU E. (1996) Lunar meteorite QUE94269—Pairing with QUE93069 confirmed. Lunar meteorite QUE 94281—similarity with Y-793274 (abstract). *Lunar Planet. Sci.* **27,** 343–344.

FUKUOKA T. (1990) Chemistry of Yamato-793274 lunar meteorite (abstract). *Symp. Antarct. Meteorites* **15th,** 122–123.

HEAD J. W., MUSTARD J., ANTONENKO I. AND HAWKE B. R. (1993) Modes of formation of lunar light plains and the detection of cryptomaria deposits (abstract). *Lunar Planet. Sci.* **24,** 629–630.

HILL D. H., BOYNTON W. V. AND HAAG R. A. (1991) A lunar meteorite found outside the Antarctic. *Nature* **352,** 614–617.

JOLLIFF B. L., KOROTEV R. L. AND HASKIN L. A. (1991) A ferroan region of the lunar highlands as recorded in meteorites MAC88104 and MAC88105. *Geochim. Cosmochim. Acta* **55,** 3051–3071.

JOLLIFF B. L., KOROTEV R. L. AND HASKIN L. A. (1993) Lunar basaltic meteorites Yamato-793169 and Asuka-881757: Samples of the same low-Ti mare lava? (abstract). *Symp. Antarct. Meteorites* **18th,** 214–217.

JOLLIFF B. L., ROCKOW K. M. AND KOROTEV R. L. (1996a) QUE 94281: Shallow plutonic VLT components and highlands components (abstract). *Lunar Planet. Sci.* **27,** 615–616.

JOLLIFF B. L., ROCKOW K. M., KOROTEV R. L. AND HASKIN L. A. (1996b) Lithologic distribution and geologic history of the Apollo 17 site: The record in soils and small rock particles from the highland massifs. *Meteorit. Planet. Sci.* **31,** 116–145.

KOEBERL C., WARREN P. H., LINDSTROM M. M., SPETTEL B. AND FUKUOKA T. (1989) Preliminary examination of the Yamato-86032 lunar meteorite: II. Major and trace element chemistry. *Proc. NIPR Symp. Antarct. Meteorites* **2,** 15–24.

KOEBERL C. K., KURAT G. AND BRANDSTÄTTER (1991) Lunar meteorite Yamato-793274: Mixture of mare and highland components, and barringerite from the Moon. *Proc. NIPR Symp. Antarct. Meteorites* **4,** 33–55.

KOEBERL C. K., KURAT G. AND BRANDSTÄTTER (1993) Gabbroic lunar mare meteorites Asuka-881757 (Asuka-31) and Yamato-793169: Geochemical and mineralogical study. *Proc. NIPR Symp. Antarct. Meteorites* **6,** 14–34.

KOROTEV R. L. (1981) Compositional trends in Apollo 16 soils. *Proc. Lunar Planet. Sci. Conf.* **12th,** 577–605.

KOROTEV R. L. (1991) Geochemical stratigraphy of two regolith cores from the Central Highlands of the Moon. *Proc. Lunar Planet. Sci. Conf.* **21st,** 229–289.

KOROTEV R. L. (1994) Compositional variation in Apollo 16 impact-melt breccias and inferences from the geology and bombardment history of the Central Highlands of the Moon. *Geochim. Cosmochim. Acta* **58,** 3931–3969.

KOROTEV R. L. (1996a) A self-consistent compilation of elemental concentration data for 93 geochemical reference samples. *Geostandards Newsletter* **20,** 217–245.

KOROTEV R. L. (1996b) On the relationship between the Apollo 16 ancient regolith breccias and feldspathic fragmental breccias, and the composition of the prebasin crust in the central highlands of the Moon. *Meteorit. Planet. Sci.* **31,** 403–412.

KOROTEV R. L. (1997) Some things we can infer about the Moon from the composition of the Apollo 16 regolith. *Meteorit. Planet. Sci.* **32,** 447–478.

KOROTEV R. L. AND KREMSER D. T. (1992) Compositional variations in Apollo 17 soils and their relationship to the geology of the Taurus-Littrow site. *Proc. Lunar Planet. Sci. Conf.* **22nd,** 275–301.

KOROTEV R. L., LINDSTROM M. M., LINDSTROM D. J. AND HASKIN L. A. (1983) Antarctic Meteorite ALHA81005—Not just another lunar anorthositic norite. *Geophys. Res. Lett.* **10,** 829–832.

KOROTEV R. L., JOLLIFF B. L. AND ROCKOW K. M. (1996) Lunar meteorite Queen Alexandra Range 93069 and the iron concentration of the lunar highlands surface. *Meteorit. Planet. Sci.* **31,** 909–924.

KRING D. A., HILL D. H. AND BOYNTON W. V. (1996) A glass-rich view of QUE 94281 (abstract). *Lunar Planet. Sci.* **27,** 707–708.

LAUL J. C., SMITH M. R. AND SCHMITT R. A. (1983) ALHA 81005 meteorite: Chemical evidence for lunar highlands origin. *Geophys. Res. Lett.* **10,** 825–828.

LINDSLEY D. H. AND ANDERSON D. J. (1983) A two-pyroxene thermometer. *Proc. Lunar Planet. Sci. Conf.* **13th,** A887–A906.

LINDSTROM D. J., WENTWORTH S. J., MARTINEZ R. R. AND MCKAY D. S. (1994) Trace element identification of three chemically distinct very low titanium (VLT) basalt glasses from Apollo 17. *Geochim. Cosmochim. Acta* **58,** 1367–1375.

LINDSTROM M. M., MARVIN U. B., HOLMBERG B. B. AND MITTLEFEHLDT D. W. (1990) Apollo 15 KREEP-poor impact melts. *Proc. Lunar Planet. Sci. Conf.* **20th,** 77–90.

LINDSTROM M. M., MITTLEFEHLDT D. W. AND MARTINEZ R. R. (1991a) Geochemistry of Asuka-31: Comparison to basaltic lunar meteorites and mare basalts (abstract). *Symp. Antarct. Meteorites* **16,** 102–105.

LINDSTROM M. M., MITTLEFEHLDT D. W., MARTINEZ R. R., LIPSCHUTZ M. E. AND WANG M-S. (1991b) Geochemistry of Yamato-82192, -86032 and -793274 lunar meteorites. *Proc. NIPR Symp. Antarct. Meteorites* **4,** 12–32.

LINDSTROM M. M., MITTLEFEHLDT D. W., MORRIS R. V. AND MARTINEZ R. R. (1996) QUE 94281, a glassy basalt-rich lunar meteorite similar to Y-793274 (abstract). *Lunar Planet. Sci.* **27,** 761–762.

LONGHI J. (1982) Effects of fractional crystallization and cumulus processes on mineral composition trends of some lunar and terrestrial rock series. *Proc. Lunar Planet. Sci. Conf* **13th,** A54–A64.

LONGHI J. (1986) Fractional crystallization of ultramafic mare magmas (abstract). *Lunar Planet. Sci.* **17,** 490–491.

LUCEY P. G., TAYLOR G. J. AND MALARET E. (1995) Abundance and distribution of iron on the Moon. *Science* **268,** 1150–1153.

NISHIIZUMI K. AND CAFFEE M. W. (1996) Exposure histories of lunar meteorites Queen Alexandra Range 94281 and 94269 (abstract). *Lunar Planet. Sci.* **27,** 959–960.

PAPIKE J. J. AND VANIMAN D. T. (1978) Luna 24 ferrobasalts and the mare basalt suite: Comparative chemistry, mineralogy, and petrology. *Mare Crisium: The View From Luna 24, GCA Suppl.* **9,** 371–401.

PIETERS C. M. (1978) Mare basalt types on the front side of the moon: A summary of spectral reflectance data. *Proc. Lunar Planet. Sci. Conf.* **9th,** 2825–2849.

SCORE R., LINDSTROM M. AND MASON B. (1995) QUE 94281: Macroscopic description (Score and Lindstrom); Thin Section (,4) Description (Mason). *Antarctic Meteorite Newsletter* **18,** 21.

STEELE A. M., COLSON R. O., KOROTEV R. L. AND HASKIN L. A. (1992) Apollo 15 green glass: Compositional distribution and petrogenesis. *Geochim. Cosmochim. Acta* **56,** 4075–4090.

TAKEDA H., MORI H. AND SAITO J. (1991a) Crystallization and brecciation histories of lunar mare meteorites, Yamato-793274 and EET87521 (abstract). *Symp. Antarct. Meteorites* **16th,** 93–95.

TAKEDA H., SAITO J., YANAI K. AND KOJIMA H. (1991b) Consortium reports of lunar meteorite Yamato-793274. *Proc. NIPR Symp. Antarct. Meteorites* **4,** 3–11.

TAYLOR G. J., WARREN P., RYDER G., DELANO J., PIETERS C. AND LOFGREN G. (1991) Chapter 6: Lunar Rocks. In *Lunar Sourcebook: A User's Guide to the Moon* (eds. G. H. Heiken, D. T. Vaniman, and B. M. French), pp. 183–284. Cambridge University Press, Cambridge, U.K.

VANIMAN D. T. AND PAPIKE J. J. (1977) Very low Ti (VLT) basalts: A new mare rock type from the Apollo 17 drill core. *Proc. Lunar Sci. Conf.* **8th,** 1443–1471.

WARREN P. H. (1989) KREEP: Major-element diversity, trace-element uniformity (almost). In *Workshop on Moon in Transition: Apollo 14, KREEP, and Evolved Lunar Rocks*, pp. 149–153. Lunar and Planetary Institute, Houston, Texas, USA.

WARREN P. H. (1994) Lunar and Martian meteorite delivery services. *Icarus* **111,** 338–363.

WARREN P. H. AND ARAI T. (1997) Mare components in mare-highland lunar meteorite regolith breccias: Implications vis-à-vis source-crater pairing (abstract). *Lunar Planet. Sci.* **28,** 1499–1500.

WARREN P. H. AND KALLEMEYN G. W. (1991) Geochemical investigation of five lunar meteorites: Implications for the composition, origin and evolution of the lunar crust. *Proc. NIPR Symp. Antarct. Meteorites* **4,** 91–117.

WARREN P. H. AND KALLEMEYN G. W. (1993) Geochemical investigation of two lunar meteorites: Yamato-793169 and Asuka-881757. *Proc. NIPR Symp. Antarct. Meteorites* **6,** 35–57.

WENTWORTH S., TAYLOR G. J., WARNER R. D., KEIL K., MA M-S. AND SCHMITT R. A. (1979) The unique nature of Apollo 17 VLT mare basalts. *Proc. Lunar Planet Sci. Conf.* **10th,** 207–223.

YANAI K. AND KOJIMA H. (1990) Varieties of the lunar meteorites collected from Antarctica (abstract). *Symp. Antarct. Meteorites* **15th,** 129–130.

YANAI K. AND KOJIMA H. (1991) Varieties of lunar meteorites recovered from Antarctica. *Proc. NIPR Symp. Antarct. Meteorites* **4,** 70–90.

APPENDIX

The appendix appears on the following pages.

TABLE A1. Compositions of subsamples of the QUE 94281 lunar meteorite by instrumental neutron activation analysis.

Sample Number	Lab #	Na_2O	CaO	Sc	Cr	FeO	Co	Ni	Rb	Sr	Zr	Cs	Ba	La	Ce	Nd	Sm
QUE 94281,34A	311.041	0.44	11.8	26.4	1957	12.91	53.9	490	6	160	110	<0.21	75	6.86	18.7	11	3.27
QUE 94281,34B	311.042	0.36	12.7	28.9	1637	13.19	45.5	280	<13	130	130	<0.23	66	7.06	18.9	11	3.34
QUE 94281,34C	311.043	0.39	12.9	29.1	1618	13.27	46.4	340	<12	120	120	<0.3	87	7.96	21.4	12	3.80
QUE 94281,34D	311.044	0.39	13.1	29.9	1707	13.54	47.6	350	8	120	120	<0.22	90	7.53	20.4	14	3.56
QUE 94281,34E	311.045	0.38	13.2	30.0	1681	13.55	47.3	390	<10	120	130	0.10	83	7.37	19.5	12	3.52
QUE 94281,35A1	311.046	0.56	14.3	10.4	723	5.24	13.2	161	4	185	174	0.15	141	11.8	30.7	18	5.35
QUE 94281,35A2	311.047	0.45	13.4	23.3	1449	11.15	30.5	130	5	117	123	0.10	96	8.33	22.5	13	3.90
QUE 94281,35B	311.048	0.37	12.4	30.8	1677	14.06	41.8	170	<12	110	150	<0.3	64	7.10	19.2	10	3.49
QUE 94281,35C	311.049	0.33	11.1	35.4	2000	15.99	45.6	110	7	110	110	<0.25	69	6.05	16.1	8	2.86
QUE 94281,35D	311.050	0.35	11.6	35.3	1868	16.54	42.3	70	<11	130	130	<0.18	70	6.44	16.7	10	2.99
QUE 94281,35E	311.051	0.39	12.0	30.4	1686	13.73	40.3	130	<11	120	70	<0.3	80	6.16	16.1	8	2.80
QUE 94281,36A1	311.052	0.41	13.1	24.0	1697	11.44	47.2	430	<9	150	60	<0.19	66	6.02	16.3	9	2.82
QUE 94281,36A2	311.053	0.45	12.6	24.1	1829	12.48	60.2	610	<10	100	90	0.12	86	7.14	18.7	9	3.34
QUE 94281,36A3	311.054	0.39	13.1	29.3	2030	13.12	49.5	440	8	120	100	0.14	76	5.81	15.4	9	2.75
QUE 94281,36A4	311.055	0.41	12.7	29.0	1845	13.48	51.1	400	<9	130	80	<0.21	77	6.20	16.7	8	3.06
QUE 94281,36B1	311.056	0.41	12.3	28.2	1632	12.76	38.1	130	<10	140	100	<0.23	73	5.86	16.7	6	2.78
QUE 94281,36B2	311.057	0.40	13.4	27.4	1476	12.04	33.7	120	6	100	70	<0.16	66	6.10	15.5	10	2.83
QUE 94281,36C	311.058	0.41	13.5	28.4	1732	12.68	35.5	80	<9	80	<150	<0.3	60	6.09	16.8	9	3.06
QUE 94281,33MS3	311.059	0.42	12.2	26.0	1788	13.39	60.2	640	<12	120	140	<0.25	75	6.60	17.6	10	3.17
QUE 94281,33MS2	311.060	0.34	12.6	35.9	1945	16.00	50.1	190	<14	110	70	<0.3	65	5.81	15.6	12	3.01
QUE 94281,33MS1	311.061	0.40	13.2	30.2	1887	12.42	37.4	140	<10	80	<130	<0.22	69	5.89	15.6	10	2.80
QUE 94281,33A	311.062	0.38	12.9	29.2	1855	14.12	48.5	320	<11	100	<140	<0.22	77	5.43	14.7	<14	2.74
QUE 94281,33B	311.063	0.38	12.8	30.9	1862	13.93	48.1	300	4	120	100	<0.14	67	7.61	20.1	12	3.52
QUE 94281,33C	311.064	0.40	12.1	28.4	1905	13.89	57.8	560	5	128	120	0.11	83	6.52	17.8	9	3.15
QUE 94281,33D	311.065	0.33	11.8	34.9	2080	15.29	47.6	140	7	100	130	<0.21	57	5.92	15.9	9	2.87
QUE 94281,33E	311.066	0.39	12.9	30.1	2150	14.08	49.9	360	<11	120	<160	<0.3	70	6.01	15.7	7	2.80
QUE 94281,33F	311.067	0.41	12.3	28.4	1931	13.52	49.3	420	7	90	90	<0.24	84	6.86	18.0	12	3.23
QUE 94281,33G	311.068	0.41	12.4	27.2	1797	13.18	48.3	320	<10	120	90	<0.19	85	6.17	16.4	9	2.84
Uncertainty		0.01	0.4	0.6	40	0.3	1	35	3	30	35	0.07	12	0.14	0.3	3	0.06

Oxide concentrations are in wt%, all others in ppm except Ir and Au (ppb). All Fe reported as FeO. Uncertainty = estimated analytical precision (1σ) for a sample of average mass and composition.

TABLE A1. *Continued.*

Sample Number	Eu	Tb	Yb	Lu	Hf	Ta	Ir	Au	Th	U	Mass (mg)	Description
QUE 94281,34A	0.84	0.66	2.45	0.342	2.41	0.31	16.9	3.8	1.09	0.29	14.17	Dull gray-black glass
QUE 94281,34B	0.86	0.72	2.55	0.359	2.53	0.30	6.0	<5	1.09	0.30	17.43	Black glass, large fragment
QUE 94281,34C	0.86	0.79	2.85	0.399	2.78	0.35	11.6	<4	1.23	0.33	19.15	Black glass, two fragments
QUE 94281,34D	0.87	0.76	2.70	0.368	2.70	0.32	13.6	<5	1.15	0.29	20.07	Black glass, small fragments
QUE 94281,34E	0.86	0.75	2.64	0.362	2.52	0.33	16.0	2	1.12	0.23	17.16	Black glass, fines
QUE 94281,35A1	1.25	1.03	3.54	0.497	4.22	0.50	10.1	<4	1.86	0.48	11.82	White lithic clast fragments
QUE 94281,35A2	1.00	0.79	2.83	0.400	3.71	0.72	5.1	<3	1.31	0.26	13.55	White lithic clast plus matrix
QUE 94281,35B	0.83	0.76	2.66	0.378	3.97	0.45	5.2	<3	1.07	0.35	12.25	Bulk breccia
QUE 94281,35C	0.75	0.63	2.34	0.324	2.88	0.27	<7	<3	0.99	0.28	12.48	Bulk breccia
QUE 94281,35D	0.77	0.66	2.62	0.374	2.91	0.37	<8	<3	1.05	0.24	8.44	Bulk breccia
QUE 94281,35E	0.83	0.59	2.21	0.307	2.33	0.29	8	3.8	0.98	0.25	14.98	Bulk breccia
QUE 94281,36A1	0.84	0.56	2.08	0.290	1.85	0.21	13.5	4.5	0.91	0.22	13.39	Mostly breccia plus white clasts
QUE 94281,36A2	0.85	0.74	2.48	0.335	2.50	0.33	18.4	3.5	0.98	0.29	18.78	Mostly black, vesicular glass
QUE 94281,36A3	0.81	0.56	2.19	0.302	2.11	0.31	17	5.3	0.85	0.27	20.76	Black glass plus breccia
QUE 94281,36A4	0.82	0.65	2.28	0.325	2.22	0.46	11.9	3.8	0.95	0.23	10.33	Black glass plus breccia, fines
QUE 94281,36B1	0.86	0.58	2.16	0.301	2.35	0.31	4.0	<4	1.10	0.21	15.12	Bulk breccia
QUE 94281,36B2	0.85	0.63	2.18	0.305	2.43	0.29	4.2	<4	1.01	0.21	16.50	Bulk breccia
QUE 94281,36C	0.89	0.67	2.36	0.340	2.20	0.26	<7	<5	0.94	0.20	20.32	Bulk breccia, clast-rich, fragments
QUE 94281,33MS3	0.82	0.68	2.47	0.344	2.57	0.33	26	6.7	0.96	0.26	15.77	Bulk breccia, most magnetic, glass-rich
QUE 94281,33MS2	0.69	0.71	2.60	0.360	2.36	0.27	9.2	4.3	0.88	0.28	26.85	Bulk breccia, interm. magnetic, pyroxene-rich
QUE 94281,33MS1	0.84	0.61	2.16	0.304	2.26	0.26	6.3	<5	0.94	0.22	28.89	Bulk breccia, least magnetic
QUE 94281,33A	0.80	0.60	2.27	0.320	2.17	0.26	13	2.8	0.80	0.17	20.09	Bulk breccia, clast-rich, with glass veins
QUE 94281,33B	0.82	0.73	2.50	0.327	2.31	0.29	10.0	3.1	1.09	0.39	18.16	Bulk breccia, clast-rich
QUE 94281,33C	0.83	0.67	2.40	0.339	2.80	0.35	19.0	7	1.01	0.31	14.69	Bulk breccia, clast-rich, with vesicular glass rim
QUE 94281,33D	0.73	0.65	2.25	0.314	2.15	0.28	5.3	<5	0.81	0.19	14.41	Bulk breccia, clast-rich, with vesicular glass rim
QUE 94281,33E	0.78	0.62	2.25	0.316	2.00	0.28	12	3.5	0.90	0.20	18.78	Bulk breccia, clast-rich, with glass veins
QUE 94281,33F	0.85	0.67	2.44	0.337	2.33	0.30	13.2	5.7	1.02	0.25	14.73	Bulk breccia, with vesicular black glass
QUE 94281,33G	0.84	0.61	2.36	0.341	2.31	0.30	11.5	3.9	1.08	0.24	14.63	Bulk breccia, with yellow clasts, glass, and fines
Uncertainty	0.03	0.03	0.05	0.007	0.07	0.04	1.7	1.2	0.04	0.06		

Oxide concentrations are in wt%, all others in ppm except Ir and Au (ppb). All Fe reported as FeO. Uncertainty = estimated analytical precision (1σ) for a sample of average mass and composition.

TABLE A2. Compositions of pyroxene clasts of "VLT trend" in QUE 94281 lunar meteorite by electron-microprobe analysis.

	Px 22	Px 6	Px 29	Px 23	Px 32	Px 8	Px 27	Px 20	Px 13	Px 15	Px 3	Px 9	Px 18	Px 7	Px 17	Px 26
n	2	2	2	1	1	2	1	2	1	3	3	2	1	2	2	2
SiO_2	52.7	53.2	52.6	51.9	52.8	52.1	51.0	51.4	51.4	51.9	51.1	51.6	51.0	50.3	50.1	49.7
TiO_2	0.21	0.18	0.17	0.27	0.17	0.22	0.31	0.29	0.30	0.25	0.27	0.35	0.34	1.10	0.55	0.45
Al_2O_3	1.45	1.38	1.37	1.74	1.36	1.53	1.83	1.48	1.68	1.39	1.44	1.87	1.36	2.13	1.41	1.23
Cr_2O_3	0.65	0.64	0.65	0.75	0.65	0.68	0.72	0.71	0.66	0.65	0.53	0.52	0.53	0.32	0.49	0.44
FeO	16.7	17.3	19.2	14.5	19.1	18.8	15.4	19.5	16.2	20.7	19.7	18.8	18.3	22.2	21.9	25.1
MnO	0.28	0.30	0.30	0.26	0.35	0.33	0.22	0.33	0.22	0.34	0.34	0.36	0.33	0.37	0.32	0.32
MgO	21.5	21.6	20.0	15.1	18.8	18.4	14.0	17.7	13.9	17.6	15.6	14.7	13.6	14.9	11.2	11.5
CaO	6.02	5.30	6.00	15.4	6.54	7.52	15.9	7.93	15.3	6.98	10.1	11.4	14.2	7.90	13.4	10.8
Na_2O	0.04	0.03	0.00	0.04	0.03	0.02	0.04	0.03	0.03	0.02	0.02	0.03	0.04	0.09	0.07	0.06
Total	99.5	100.0	100.2	99.9	99.8	99.5	99.4	99.3	99.6	99.8	99.1	99.7	99.6	99.3	99.4	99.6
Mg'	69.7	69.0	65.1	64.9	63.6	63.5	61.9	61.8	60.5	60.2	58.6	58.2	57.0	54.6	47.7	44.9
Ti/(Ti + Cr)	0.24	0.21	0.19	0.26	0.21	0.24	0.29	0.28	0.30	0.27	0.33	0.39	0.38	0.77	0.51	0.49
Wo	13.0	12.2	12.8	29.0	13.7	17.1	30.3	17.3	29.3	16.2	22.3	26.4	27.8	20.6	26.9	24.2
En	60.6	60.6	56.7	46.1	54.9	52.7	43.2	51.1	42.7	50.5	45.6	42.8	41.2	43.3	34.9	34.0
Fs	26.4	27.2	30.4	24.9	31.4	30.2	26.6	31.6	27.9	33.4	32.2	30.8	31.1	36.1	38.2	41.8

	Px 2	Px 5	Px 19	Px 24	Px 14	Px 21	Px 12	Px 25	Px 4	Px 10	Px 11	Px 28	Px 31	Px 16	Px 30	Px 1
n	2	2	1	3	1	3	4	1	4	3	4	2	1	1	1	2
SiO_2	50.9	50.0	49.4	49.7	49.7	49.4	49.2	49.1	49.4	48.6	49.0	48.5	48.6	48.6	49.2	46.7
TiO_2	0.34	0.75	0.49	0.56	0.35	0.63	0.61	0.65	0.79	0.68	0.68	1.00	0.81	0.95	1.01	1.24
Al_2O_3	1.00	0.78	0.96	1.00	0.94	1.18	1.07	1.18	1.13	1.48	0.97	0.87	0.78	1.09	0.89	1.07
Cr_2O_3	0.35	0.00	0.33	0.34	0.35	0.37	0.36	0.33	0.31	0.32	0.21	0.12	0.11	0.12	0.08	0.04
FeO	27.7	25.7	28.4	27.7	29.1	25.5	28.1	25.9	26.6	29.1	30.4	28.8	34.0	26.4	27.8	31.0
MnO	0.42	0.31	0.41	0.42	0.41	0.37	0.42	0.37	0.39	0.41	0.44	0.34	0.45	0.33	0.29	0.35
MgO	12.1	11.0	11.7	10.9	11.4	9.8	10.5	9.50	8.59	8.21	8.01	7.04	7.37	5.56	3.03	0.73
CaO	7.61	10.9	7.24	9.02	7.08	12.5	8.92	12.7	12.8	10.7	10.3	13.0	7.64	16.3	18.1	18.4
Na_2O	0.03	0.08	0.04	0.05	0.02	0.06	0.04	0.08	0.05	0.05	0.04	0.06	0.05	0.08	0.09	0.05
Total	100.5	99.5	99.1	99.7	99.4	99.8	99.2	99.8	100.1	99.5	100.0	99.7	99.9	99.5	100.5	99.6
Mg'	43.7	43.2	42.4	41.2	41.1	40.7	39.8	39.5	36.5	33.4	31.9	30.3	27.9	27.3	16.2	4.0
Ti/(Ti + Cr)	0.48	0.99	0.59	0.61	0.49	0.62	0.62	0.65	0.71	0.67	0.75	0.89	0.88	0.88	0.92	0.97
Wo	19.0	25.4	17.5	21.6	17.2	25.8	21.5	26.5	26.7	25.7	24.8	27.9	17.2	35.1	38.8	41.0
En	35.4	32.3	35.0	32.3	34.0	30.2	31.3	29.1	26.8	24.8	24.0	21.9	23.1	17.7	9.9	2.4
Fs	45.6	42.3	47.5	46.2	48.8	44.0	47.2	44.4	46.6	49.5	51.1	50.3	59.7	47.2	51.3	56.6

Compositions are sorted by *Mg'* (atomic Mg/[Mg + Fe] × 100). Those for which n > 1 are averages of *n* analyses. Beam size ranged from 10 to 30 μm.
Wo, En, and Fs calculated on the basis of 6 O atoms and "corrected" for jadeite, CrCaTs, and AlCaTs components. Total Fe given as FeO.

TABLE A3. Compositions of plagioclase clasts in QUE 94281 by electron-microprobe analysis.

	Pl 19	Pl 16	Pl 4	Pl 12 (Px32)	Pl 9	Pl 22 (Px31)	Pl 11	Pl 5	Pl 18	Pl 1	Pl 14
SiO_2	44.2	43.8	43.8	44.5	43.2	44.7	44.6	44.3	44.2	44.4	45.2
Al_2O_3	36.4	35.7	35.1	35.2	34.7	35.3	35.1	35.2	35.5	35.5	34.2
FeO	0.12	0.08	0.39	0.34	0.26	0.36	0.32	0.24	0.23	0.22	0.51
MgO	0.02	0.08	0.10	0.09	0.02	0.02	0.06	0.06	0.02	0.03	0.23
CaO	19.3	19.3	19.2	19.2	18.5	18.3	18.9	18.6	18.6	18.8	18.5
Na_2O	0.42	0.46	0.62	0.65	0.67	0.72	0.76	0.76	0.78	0.79	0.88
K_2O	0.01	0.08	0.01	0.02	0.03	0.04	0.02	0.02	0.05	0.04	0.00
Total	100.5	99.5	99.1	100.0	97.3	99.4	99.8	99.2	99.4	99.8	99.6
An	96.1	95.4	94.4	94.1	93.7	93.1	93.1	93.0	92.7	92.7	92.0
Ab	3.8	4.1	5.5	5.8	6.1	6.7	6.8	6.9	7.0	7.1	7.9
Or	0.06	0.5	0.08	0.09	0.2	0.2	0.12	0.11	0.3	0.2	0.04

	Pl 21 (Px14)	Pl 6	Pl 2	Pl 7	Pl 17	Pl 10	Pl 13	Pl 20 (Px14)	Pl 3	Pl 8	Pl 15
SiO_2	45.5	44.5	45.1	45.3	45.0	45.4	46.0	46.1	45.3	46.8	51.6
Al_2O_3	35.2	35.0	35.0	35.0	35.0	34.5	34.3	34.1	34.2	33.1	30.0
FeO	0.48	0.23	0.09	0.32	0.09	0.21	0.30	0.69	0.19	0.41	0.69
MgO	0.05	0.08	0.12	0.06	0.10	0.08	0.04	0.07	0.09	0.05	0.02
CaO	18.1	18.5	18.6	18.5	18.7	18.1	18.0	17.5	17.7	16.8	13.8
Na_2O	0.87	0.91	0.87	0.96	0.97	1.04	1.26	1.29	1.37	1.74	3.15
K_2O	0.02	0.02	0.13	0.03	0.05	0.04	0.11	0.02	0.05	0.16	0.54
Total	100.2	99.3	100.0	100.1	99.9	99.3	100.1	99.7	98.8	99.1	99.8
An	91.9	91.7	91.5	91.2	91.1	90.3	88.2	88.1	87.5	83.4	68.3
Ab	8.0	8.2	7.7	8.6	8.6	9.4	11.2	11.8	12.3	15.6	28.3
Or	0.12	0.14	0.8	0.15	0.3	0.2	0.6	0.12	0.3	0.9	3.2

Analyses are listed in order of decreasing An content. An, Ab, and Or calculated from cation proportions on the basis of eight oxygen atoms. (Px#) indicates the corresponding pyroxene analysis (Table A2) for composite pyroxene-plagioclase grains.

TABLE A4. Compositions of olivine clasts in QUE 94281 by electron-microprobe analysis.

	Ol 10 (Px22)	Ol 9 (Px22)	Ol 12	Ol 3 (Px17)	Ol 5	Ol 13	Ol 1 (Px7)	Ol 4	Ol 8	Ol 6	Ol 11 (Px16)	Ol 7	Ol 2
SiO_2	36.6	37.0	38.0	36.6	36.7	36.6	35.7	34.1	32.8	32.9	30.9	30.1	30.4
TiO_2	0.03	<0.02	0.04	0.03	0.55	0.06	0.11	0.07	0.05	0.24	0.09	0.12	0.11
Al_2O_3	0.08	<0.01	0.15	0.00	0.46	0.06	0.13	0.09	<0.01	1.51	<0.01	<0.01	<0.01
Cr_2O_3	0.08	0.08	0.07	0.06	0.04	0.03	0.02	0.06	0.07	0.02	<0.02	0.02	<0.02
FeO	30.6	30.9	32.0	33.1	33.5	36.2	41.0	45.2	53.8	56.0	62.4	65.5	66.5
MnO	0.33	0.33	0.24	0.34	0.34	0.41	0.40	0.43	0.47	0.56	0.64	0.68	0.75
MgO	31.8	31.9	30.3	29.6	27.9	27.1	22.4	19.2	12.9	6.98	4.91	2.66	1.55
CaO	0.09	0.12	0.18	0.16	0.65	0.20	0.41	0.39	0.32	1.68	0.33	0.45	0.54
Na_2O	<0.01	<0.01	0.01	0.00	<0.01	0.01	<0.01	0.03	<0.01	0.04	<0.01	0.00	0.02
Total	99.6	100.3	101.0	99.9 avg (2)	100.1	100.6	100.2	99.6	100.4	100.0	99.3	99.6 avg (2)	99.9
Mg'	64.9	64.8	62.8	61.5	59.7	57.2	50.7	43.1	29.9	18.2	12.3	6.7	4.0

Compositions are sorted by *Mg'* (atomic Mg/[Mg + Fe] × 100). Total Fe given as FeO. (Px#) indicates the corresponding pyroxene analysis (Table A2) for composite pyroxene-olivine grains. Compositions for Ol 5 and Ol 6 might appear, from high Al_2O_3 concentrations, to be affected by overlap of the beam onto plagioclase, but the grains are coarse enough that this should not be the case; also, the Al_2O_3/CaO values would be higher than they are if there was beam overlap onto plagioclase.

TABLE A5. Compositions of coexisting minerals in selected QUE 94281 lithic clasts by electron-microprobe analysis.

	Lithic Clast 1			Lithic Clast 2						Lithic Clast 3			Lithic Clast 4	
	Ol 1	Ol 2	Plag 1	Px 1	Px 2	Ol 1	Plag 1	Plag 2	Plag 3	Ol 1	Px 1	Plag 1	Px 1	Ol 1
SiO_2	37.6	37.4	43.6	50.8	54.6	40.2	52.5	43.9	52.3	36.9	50.3	43.9	48.6	30.6
TiO_2	0.07	0.07	0.05	2.51	0.62	0.03	0.14	0.13	0.14	0.06	1.80	0.05	0.81	0.18
Al_2O_3	0.05	0.00	34.5	3.05	0.80	0.27	29.0	35.2	30.2	0.00	2.32	34.5	1.05	0.01
Cr_2O_3	0.14	0.03	0.00	0.32	0.11	0.03	0.02	0.00	0.02	0.08	0.63	<0.01	0.20	0.01
FeO	26.3	27.2	0.18	7.76	12.1	18.3	0.22	0.35	0.24	31.6	10.0	0.53	26.6	61.9
MnO	0.24	0.26	–	0.20	0.24	0.17	0.01	0.03	0.02	0.25	0.18	<0.01	0.43	0.67
MgO	34.8	35.1	0.11	16.1	27.1	41.8	0.23	0.10	0.20	30.4	14.5	0.28	6.00	5.27
CaO	0.08	0.10	18.7	18.9	3.85	0.05	12.5	18.8	13.2	0.22	18.7	18.8	15.5	0.19
Na_2O	–	–	0.68	0.27	0.05	0.00	4.07	0.48	3.92	–	0.13	0.55	0.06	–
K_2O	–	–	0.09	–	–	–	0.16	0.01	0.16	–	–	0.04	–	–
Total	99.3	100.1	97.9	99.8	99.4	100.9	98.8	99.1	100.4	99.4	98.6	98.7	99.2	98.8
An (Plag)	93.8	62.9	95.6	64.3	95.0									
Mg'	70.2	69.7		78.7	80.0	80.3				63.2	72.1		28.7	13.2
Wo (Px)				36.9	8.8						37.1		33.2	
En (Px)				49.7	73.0						45.4		19.1	
Fs (Px)				13.4	18.2						17.6		47.6	

Lithic Clast 1: fine-grained, granulitic texture; olivine granules in polygranular plagioclase matrix, plus whitlockite (Fig. 3e).
Lithic Clast 2: 100–200 μm grainsize polymict assemblage of plagioclase-pyroxene-olivine-ilmenite.
Lithic Clast 3: intergranular texture, feldspathic basalt; plagioclase-pyroxene-olivine-ilmenite (Fig. 3f).
Lithic Clast 4: ~200 μm, strongly fractured clast containing a vermicular intergrowth of olivine in pyroxene.